THESIS

NUMERICAL MODEL OF SEDIMENT TRANSPORT IN SEDIMENT BYPASS TUNNELS: INFLUENCE OF TRANSVERSE SLOPE IN TUNNEL BEND

Submitted By

Jesse Brown

Department of Civil and Environmental Engineering

In partial fulfillment of the requirements

For the Degree of Master of Science

Colorado State University

Fort Collins, Colorado

Spring 2025

Master's Committee:

Advisor: Christopher I. Thornton
Co-Advisor: Robert Ettema

Ciprian Dumitrache

ABSTRACT

NUMERICAL MODEL OF SEDIMENT TRANSPORT IN SEDIMENT BYPASS TUNNELS: INFLUENCE OF TRANSVERSE SLOPE IN TUNNEL BEND

Sediment Bypass Tunnels (SBTs) convey sediment around reservoirs, increasing reservoir lifespan by greatly reducing reservoir sedimentation and, thereby, mitigating consequent loss of reservoir water-storage capacity. To keep SBTs small and economical in cross-section, SBTs convey super-critical flows. Consequently, SBTs convey super-critical flows with large sediment loads, typically containing high concentrations of coarse particles of sediment that can cause abrasion of SBT liners. Especially vulnerable are SBT reaches where secondary currents develop, notably SBT bends. The sediment abrasion that occurs along the invert of a bend requires expensive, frequent replacement of the invert's concrete liner. Consequently, the abrasion rate of inverts and, therefore, bend flow fields are of interest to SBT designers. SBT design variables such as sediment-size distribution, invert-liner type (usually concrete), flow cross-section dimensions, tunnel slope and bend radius can affect sediment abrasion in an SBT, doing so by influencing flow field, secondary currents, and patterns of sediment abrasion.

This study focuses on sediment abrasion of SBTs:

1. The flow field generating secondary currents associated with free-surface flows along SBT bends; and
2. Banking of an SBT invert to reduce sediment abrasion.

The concept of invert-banking was proposed in personal communications with Dr. Ismail Albayrak of the Federal Institute of Technology (ETH), Zurich, Switzerland. The concept was floated during a SBT site inspection in April 2024. The problem of sediment abrasion is a problem for hydraulic structures in mountainous regions such as Switzerland and parts of the United States (e.g., Muller-Hagermann et al. 2020; Melesse et al. 2023).

The present study uses the Computational Fluid Dynamics (CFD) code *OpenFOAM* to create a numerical model of an existing SBT for which hydraulic-model and field data and observations exist. The numerical model was used with the solver *interFoam*, and the renormalization group (RNG) k-ε turbulence flow assumption, the volume of fluid (VOF) method, and a Discrete Element Model (DEM) coupling. Of focal interest in the modeling was the pattern of secondary flow in a bend whose invert had variable transverse sloping.

The prototype bend selected for this study is Switzerland's Solis SBT. The pattern of secondary flow in the bend affected the distribution of sediment across the bend's invert and, therefore, the sediment abrasion experienced by the bend. The Solis SBT, part of the sediment control system used for Solis Reservoir, was chosen for this study because of data and observations availability. Built in 2012, the invert of a bend in the Solis SBT has experienced severe abrasion owing to sediment.

This study recommends a small amount of banking in the Solis SBT and other tunnels with similar hydraulic properties. Even a 1% to 2% slope appears to have a substantial effect in distributing the sediment evenly.

ACKNOWLEDGEMENTS

Many thanks to Dr. Ismail Albayrak and Subhojit Kadia for providing their insights into this topic, and to my advisor at Colorado State University, Dr. Robert Ettema, for his encouragement and guidance in my pursuit of this topic.

TABLE OF CONTENTS

CHAPTER 1. INTRODUCTION

Sediment Bypass Tunnels (SBTs) convey sediment around reservoirs, thereby increasing reservoir lifespan by greatly reducing reservoir sedimentation and consequent loss of water-storage capacity. Typically, SBT flows use super-critical open-channel flows to transport alluvial sediment rapidly passed a reservoir and, thereby, keep SBT cross-section to an economical small size. However, because an SBT flow carries a large sediment load, typically containing high concentrations of coarse particles, abrasion of the SBT-invert's liner can be a problem. Especially vulnerable to abrasion are SBT bends, where secondary currents develop in SBT flows. Abrasion requires expensive, frequent replacement of concrete liners. SBT design variables such as sediment-size distribution, invert-liner type (usually concrete), flow cross-section dimensions, tunnel slope and bend radius can affect sediment abrasion in an SBT, doing so by influencing flow field, secondary currents, and patterns of sediment abrasion.

This study focuses on sediment abrasion of SBTs:

1. The flow field generating secondary currents associated with free-surface flows along SBT bends; and
2. Banking of an SBT invert to reduce sediment abrasion.

The concept of invert-banking was proposed in personal communications with Dr. Ismail Albayrak of the Federal Institute of Technology (ETH), Zurich, Switzerland, during a SBT site inspection in April 2024. Sediment abrasion is a problem for hydraulic structures in mountainous regions such as Switzerland and parts of the United States (e.g., Muller-Hagermann et al. 2020; Melesse et al. 2023).

Secondary currents in open-channel flows are a well-studied phenomena (e.g., Rouse 1950; Chow 1959; Henderson 1966) that occur when flow follows a curved path, such as flow in an SBT bend. Whether the flow is sub- or super-critical, the centrifugal force acting on the flow passing in a bend causes a rise in the water surface along the outside wall of the bend and a depression of the water surface along the inside wall of the bend. The water-surface rise is known as super-elevation, which is part of a helicoidal motion that may persist for many channel widths downstream. Super-elevation, ΔY, can be estimated using the relationship:

$$\Delta Y = \frac{BV^2}{gR_C} \qquad \text{(Eq. 1)}$$

in which B = channel (in SBT) top width; V = average velocity, R_C = radius of curvature to centerline; g = gravity acceleration; and the term V^2/R_C = average centrifugal acceleration. The increase in water surface around the outside bend occurs due to the change in momentum and centrifugal acceleration. This centrifugal force induces a secondary current that encourages sediment to distribute toward in the inside bend and scour on the outside bend. Conversely, in sediment bypass tunnels with a fixed bed, the sediment still accumulates on the inside bend and away from the outside bend, but the result is abrasion on the inside bend due to the sediment grinding and impacting the fixed bed.

The analysis leading to Eq. (1) shows that, as a sub- or super-critical flow passes around a channel bend having a flat invert, the filament indicating maximum flow velocity shifts toward the bend's inner bank, as indicated by Figure 1 (e.g., Henderson 1966). Invert banking (addition of a transverse slope of invert at a bend) is a common design adjustment to maintain uniformity of unit discharge along the bend. For super-critical flow without bed sediment transport, the banking has a slope such that the invert slopes down toward the inner bank of a bend. However,

for this analysis, the transverse slope is downwards toward the outside bend, because distribution of sediment particles alters flow resistance across an invert. Analyses of bend flows leading to equations such as Eq. (1) do not account for flow resistance variation. The transverse slopes that this study recommends are relatively small, consequent to the effects of lateral variation of flow resistance.

If the flow transports bed sediment, however, the invert must accommodate such transport, especially the frequent impacts of saltating bed particles. For a flat invert, the lateral distribution of that sediment transport, like unit discharge of flow, also attains a maximum toward the bend's inner bank. Further, if the transported sediment saltates (in water, at most about a particle diameter [Bagnold 1973]) along the channel's invert, abrasion of the invert can be anticipated to increase toward the bend's inner bank. Associated with saltation is a so-called dispersive stress[1] caused by the impact of a saltating particle hitting the invert (Bagnold 1966). The impact must be suitably large and frequent to begin abrading the invert. Consequently, diameter range of sediment particles, saltation mode of transport, and flow velocity are important variables. If the particle is comparatively small that it registers little impact, then little or no abrasion will occur. Conversely, if the particle were relatively large that the particle rolls along the invert then little impact occurs. A certain range of particle size and associated particle momentum is needed to abrade or indent an invert of given hardness or compressive strength (say of concrete).

[1] Usually built into the calibration of a sediment-transport formulation.

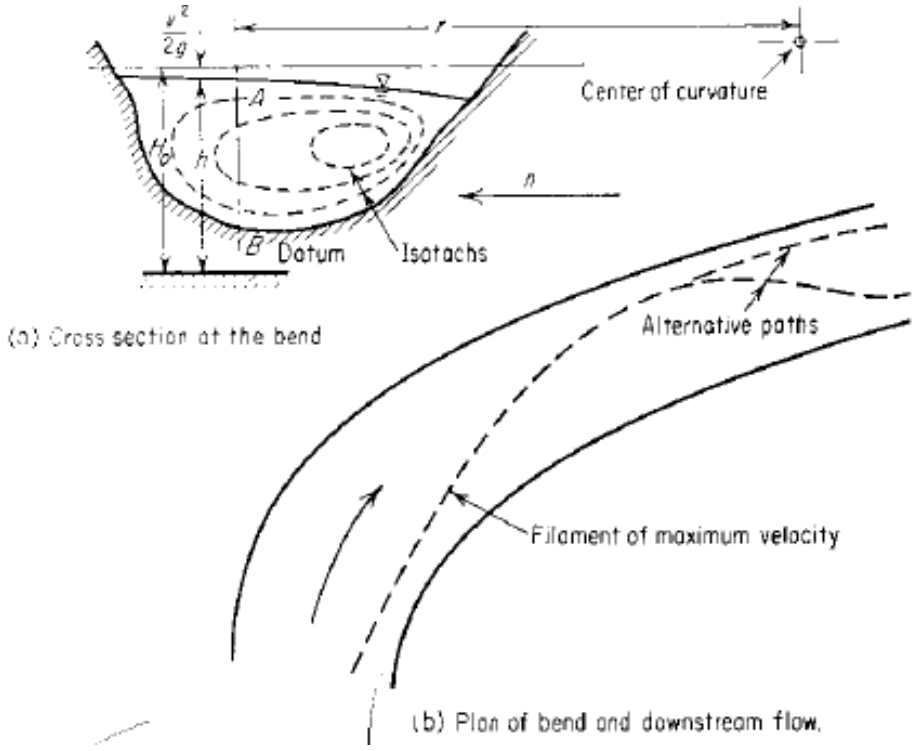

Figure 1. Flow around a channel bend: (a) vertical section; and (b) plan view (Henderson 1966*)*

The lateral shift of velocity around a bend is augmented by the generation of a secondary current directed toward the inner bank. The current forms irrespective of whether the approach flow is super- or sub-critical. The generation of a secondary current affects the transport of sediment particles, especially particles moving in saltation along the invert, as the current acts to move those particles toward the inner bank. The secondary currents in the bend may cause bedload intensity to increase near the bend's inner bank, causing invert abrasion in along the inside of a bend. This phenomenon is demonstrated in the physical modeling of the Solis SBT done by Kadia (2024). Figure 2, taken from Kadia (2024), shows the scouring zones based on a moveable bed or a fixed bed. A consequence of secondary current and particle saltation is that, at a bend, the transverse slope of an SBT invert conveying a super-critical flow may not slope downwards to the inner wall.

1.1 Objectives

This study had the following main objectives:

1. Determine how secondary currents influence the distribution of sediment in SBTs in a coupled a CFD-DEM model (computational fluid dynamics – discrete element); then (2)
2. Evaluate transverse-slope alternatives that most evenly distribute the bedload across the invert of the selected SBT.

The present study addressed these objectives by using the Computational Fluid Dynamics (CFD) code *OpenFOAM* to create a numerical model of an existing SBT for which hydraulic-model and field data and observations exist. The numerical model used the solver *interFoam*, and the renormalization group (RNG) k-ε turbulence flow assumption, the volume of fluid (VOF) method, and a Discrete Element Model (DEM) coupling.

The SBT conditions used in the numerical modeling conducted for this study use the geometry and hydraulics associated with a bend in the Solis SBT. Flow in the Solis SBT bend has been extensively modeled physically, generally studied, and the prototype SBT has been in operation for several years (Solis 2010, Kadia 2024). The Solis SBT, part of the sediment control system used for Solis Reservoir, was chosen for this study because of data and observation availability. Built in 2012, a bend in the Solis SBT has experienced severe abrasion owing to sediment.

1.2 Organization of Report

This report is organized into several sections. Chapter 2 covers the current body of knowledge of wear patterns due to secondary currents in SBTs, and the known literature for how to reduce these secondary currents. Chapter 3 covers the abrasion mechanism and sediment parameters in the modeling. Chapter 3 also covers the approach that is taken to change the model geometry to

better distribute the sediment along the SBT's invert. Chapter 4 covers the results and effectiveness of the selected approach. Chapter 5 covers the conclusions and further recommended analysis.

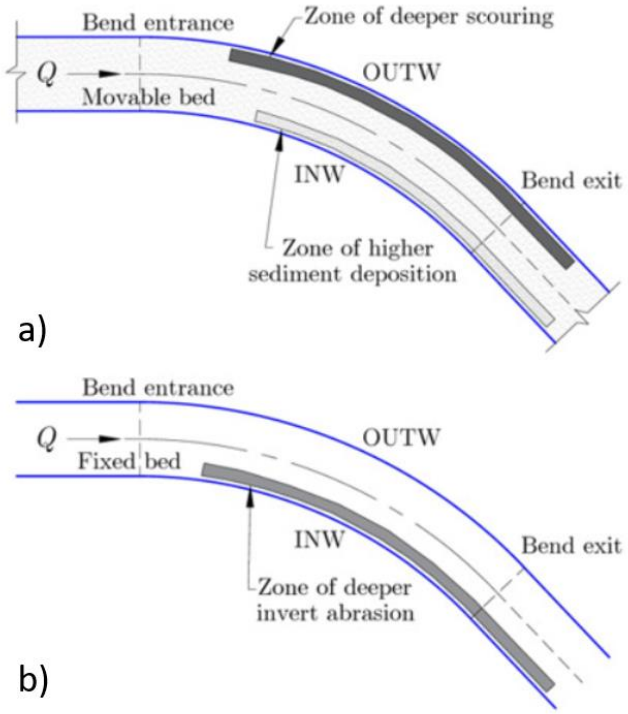

Figure 2. Conceptual sketches taken from Kadia (2024) that illustrate the sediment concentration and abrasion or scouring patterns for fixed and movable bed bends: a) plan view of the typical zones of deeper scouring and higher sediment deposition on a movable bed [based on Kawai and Julien (1996), Matsuura and Townsend (2004), and Rozovskii (1957)]; and b) plan view of the typical zone of deeper invert abrasion in sediment bypass tunnels with the fixed bed [based on Müller-Hagmann (2018), Müller-Hagmann et al. (2020), and Nakajima et al. (2015)].

CHAPTER 2. BACKGROUND AND LITERATURE REVIEW

2.1 Observed Abrasion in SBTs.

Abrasion damage induced by sediment-laden, super-critical flows has been a significant problem for hydraulic structures (e.g., Liu 2024). Abrasion damage of concrete is governed by complicated interactions between the flow, concrete, and the dynamics of moving sediment particles (Facchini 2017). Typically, the flows conveyed by SBTs are super-critical and, therefore, involve relatively high velocities. Bends in SBTs are notably complicated by the influence of centrifugal acceleration acting on a flow and, therefore, the concentration of dispersive stress exerted by a range of particle sizes.

Curvature of an SBT introduces secondary current flow patterns that in turn create dynamic forces on the sediment which then create predictable patterns of abrasion. Many SBTs require curvature, or a bend, in alignment to get around a reservoir and a dam. Figure *3* shows that it is very common for SBTs to have at least one or two bends. SBT bends are quite gradual compared to river bends, which may have a ratio of radius-of-curvature to channel width, R/B, value of about 5 (Blanckaert 2003); here R = radial distance to mid-channel, and B = channel width. The value of R/B of the Solis SBT bend is quite large, with 145 m/4.4 m = 32.95. The value of R/B is typically more gradual for SBTs than river channels, due to the necessity of controlling flow to have no separation regions in an SBT. However, although SBT bends are gradual, they can still produce strong secondary currents in super-critical flow, and these currents can impact the distribution of bedload across the invert of the SBT.

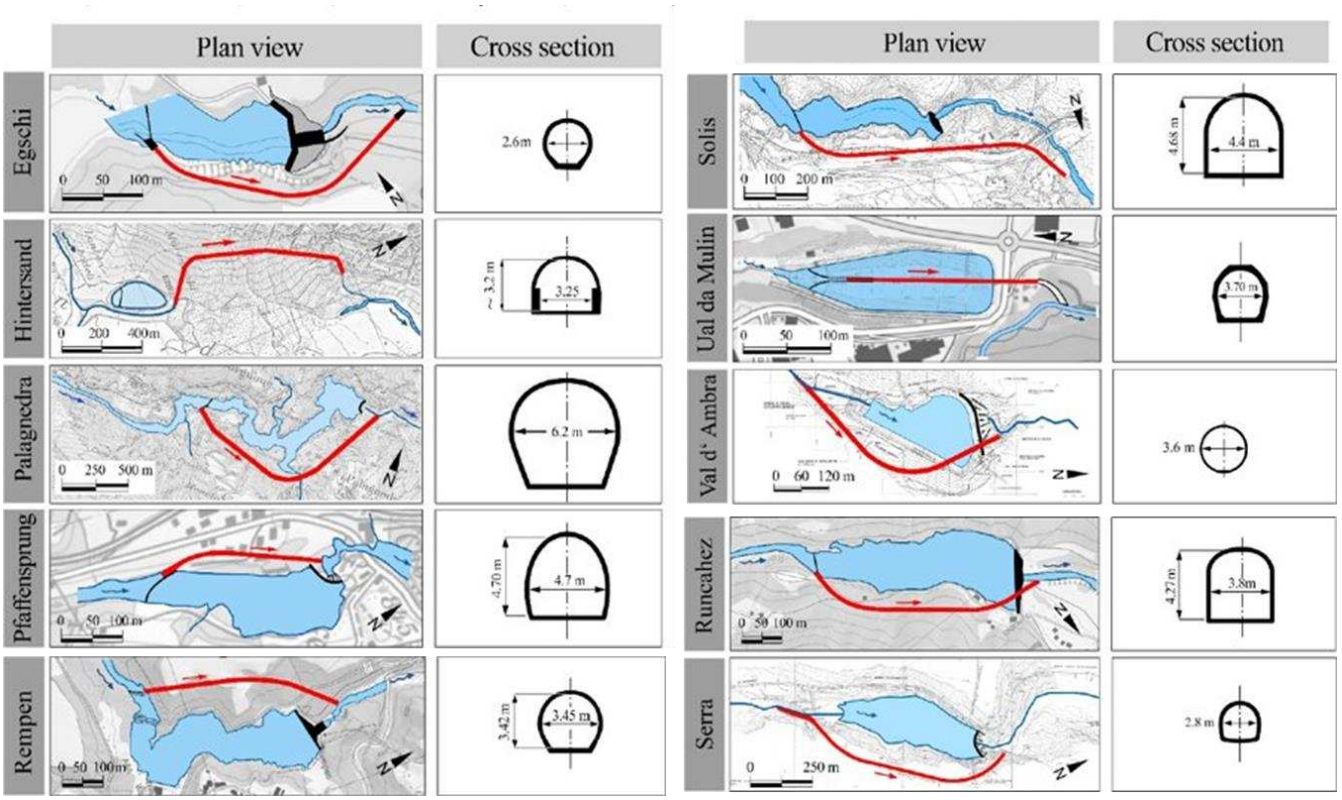

Figure 3. Plan view of existing SBTs in Switzerland, Germany, Italy, and Spain (Source, Dr. Ismail Albayrak).

Field data and observations show that the presence of bends in SBTs creates an uneven abrasion pattern in the SBT liner. The centrifugal force caused by a secondary current that forms in the bend displaces and concentrates the bedload initially uniformly distributed across the SBT invert as it approaches the bend. Figure 4, taken from Solis physical model report (Solis 2010), and Figure 5 shows bedload in the approach flow. This continual rotation and shifting of sediment toward the inside boundary of the bend creates a common pattern of abrasion, as seen along the inside of bends in several of SBTs. This pattern that has been produced consistently in SBTs such as Pfaffensprung and Solis in Switzerland, Asahi in Japan and Mud Mountain in United States (see Figure 6, Figure 7, Figure 8, and **Error! Reference source not found.**, respectively.). As can be seen in each of these figures, there is an increased abrasion rate locally

along the inside of a bend. This abrasion rate and depth exceeds values at SBT sections where the bedload is uniformly distributed across the SBT channel.

Figure 4. Sketch from Solis physical model report. The sketch shows the effect of secondary flow and primary flow on sediment transport at an SBT bend. (Solis 2010)

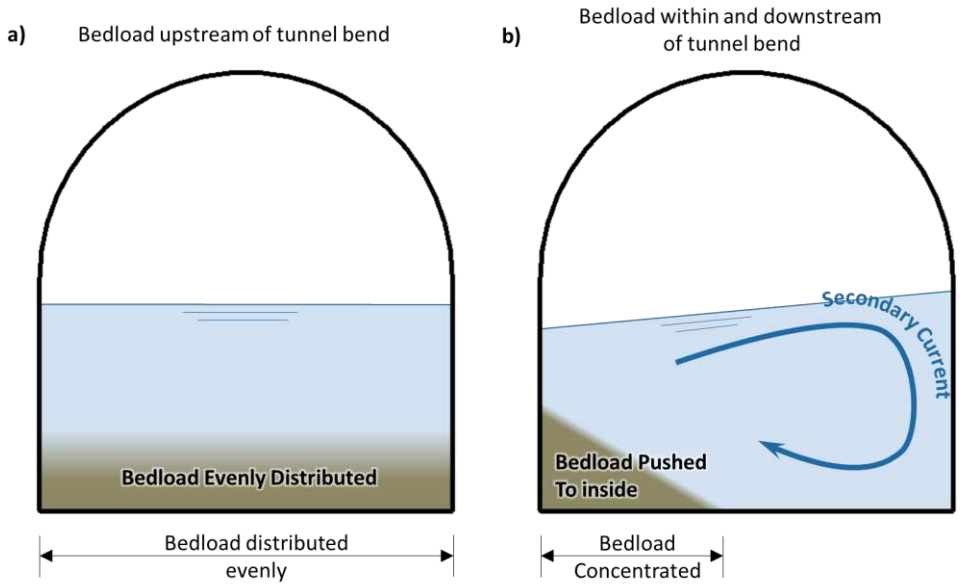

Figure 5. A conceptual sketch of bedload being moved toward the inside of a tunnel bend; (a) sediment essentially uniformly distributed along a straight approach channel; and (b) pushed toward the inner bank of an SBT bend. (Solis 2010)

Figure 6. 2024 views of abrasion observed along the inside of a bend in the SBT at Pfaffensprung, Switzerland.

Figure 7. 2024 views of abrasion observed along the inside of a bend in the SBT at Solis, Switzerland.

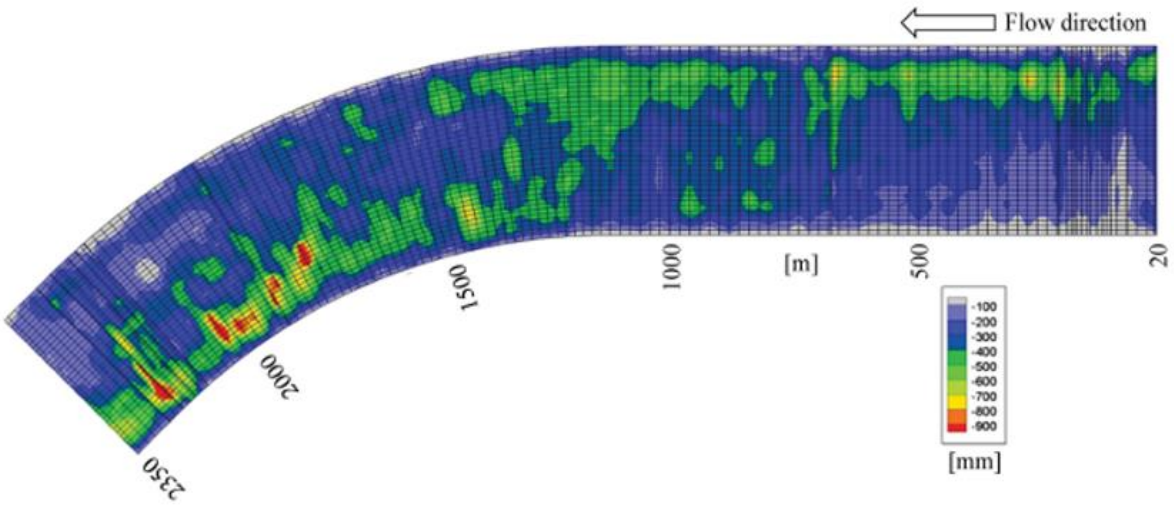

Figure 8. Cumulative abrasion pattern of a bend in the SBT at Asahi Reservoir, Japan (1998 to 2011).

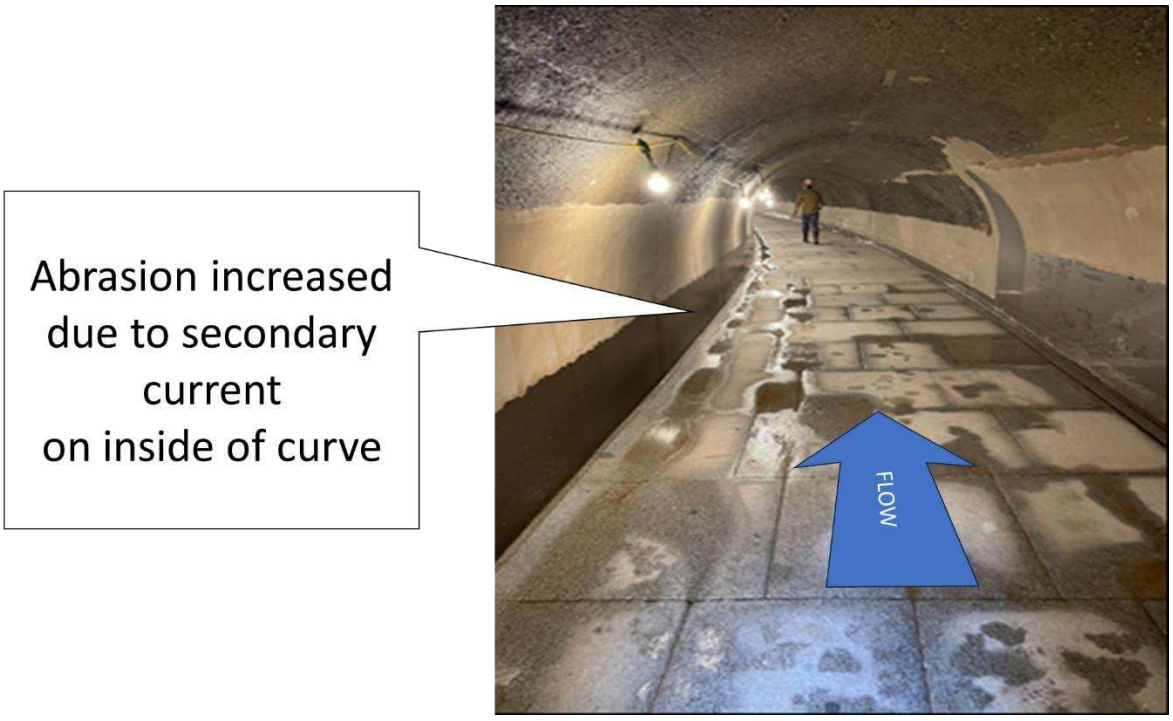

Figure 9. A 2023 view of abrasion along inside of bend Mud Mountain Dam, Washington, U.S.

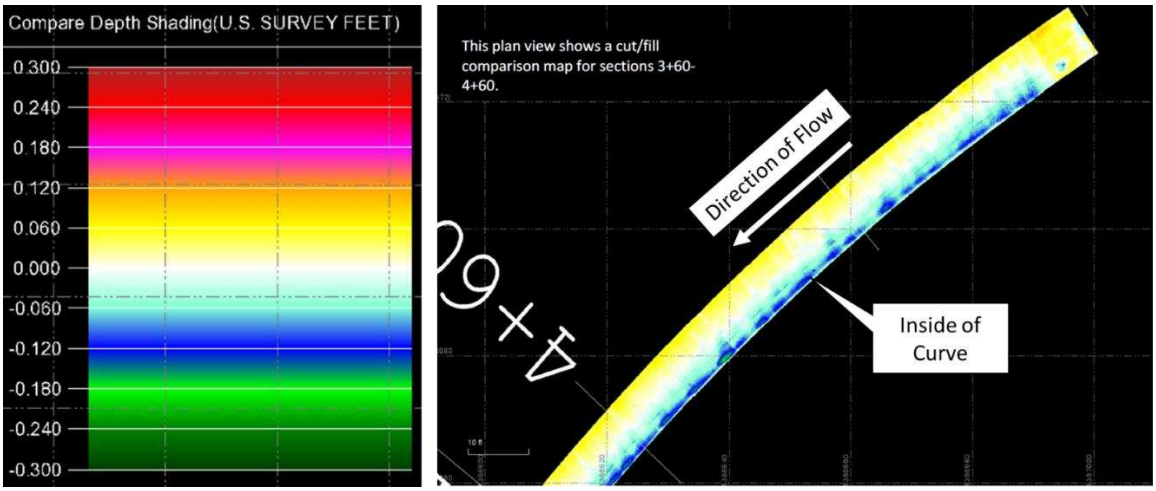

Figure 10. LiDAR-scan views of the SBT at Mud Mountain Dam, U.S. The scans were taken after five years of SBT operation and show abrasion along an inside bend.

Figure 11 shows LiDAR scan results from the SBT at Mud Mountain Reservoir. The scans show that the volume of material lost in the tunnel liner impacted by secondary currents is nearly double that of sections of the SBT that are straight and have uniform flow. From station 06+00 to 12+00 (182.9 m in length) the volume loss is 3.5 cubic meters after 5 years. However, for the sections downstream of the first curve, 00+00 to 03+00 and 03+00 to 06+00, the volume loss is 3.13 and 3.2 cubic meters, respectively, which is nearly double the loss of the straight section. The volume loss of the liner along the inside bend due to the presence of the secondary current should theoretically match the volume loss of the uniform flow section. However, this increased volume loss is not readily predicted by existing abrasion models discussed further in Section 2.2, Applicable Existing Guidance. The abrasion rate should be higher in the SBT bend due to the concentration of sediment, but the overall increase in volume loss is not well understood. For instance, in the conceptual sketch shown in Figure 12, the depths of abrasion may differ between the uniform section of flow and the section influenced by the secondary current, but the overall volume of material removed predicted by the abrasion equation should be similar. The findings

in this thesis may shed light on why there is an increased volume loss on the inside bend and lists potential hypotheses for further analysis in future studies.

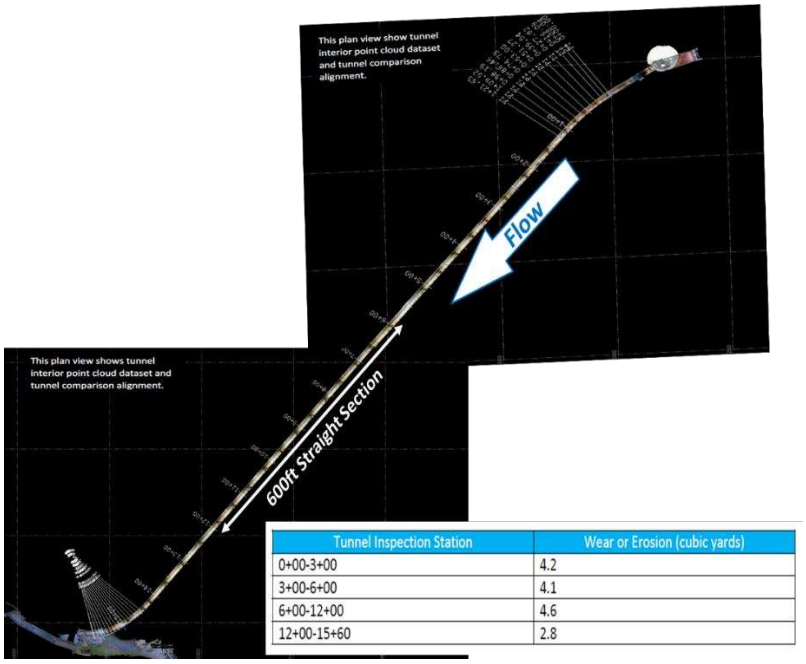

Tunnel Inspection Station	Wear or Erosion (cubic yards)
0+00-3+00	4.2
3+00-6+00	4.1
6+00-12+00	4.6
12+00-15+60	2.8

Figure 11. Straight section of Mud Mountain tunnel has 50% less abrasion than the sections that are impacted by secondary currents.

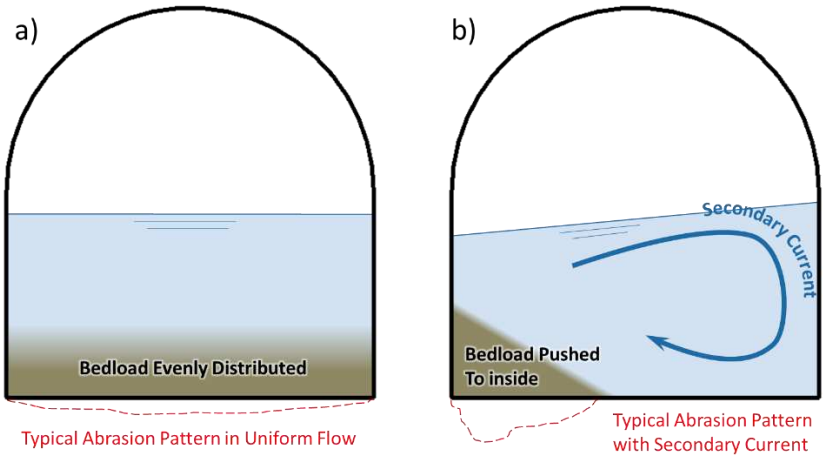

Figure 12. Conceptual sketch of abrasion patterns in tunnel sections, uniform flow and influenced by secondary current.

2.2 Applicable Existing Guidance

Several guides exist that suggest ways to greatly reduce or eliminate secondary currents in open-channel bends. One guide was suggested by the Iowa Institute of Hydraulic Research (IIHR) in 1984. Another guide is suggested by United States Army Corps of Engineers (1991), which suggests banking (transverse sloping) the invert at a bend may counter the formation of secondary currents.

A study conducted at IIHR led to a better understanding of how secondary currents influence bank erosion (Kitanidis 1984). Another study conducted addressed an underlying idea involves countering the torque exerted on the primary flow by its curvature and vertical velocity gradient, thereby eliminating or significantly reducing the secondary current which causes the un-equal distribution of sediment in the channel bottom (Odgaard 1983) and, therefore, bottom roughness. Although this concept was mainly intended for rivers conveying subcritical flow, the equation may still also be effective for super-critical flows in SBTs. However, adding features like vanes into SBTs may also create issues with disrupting the super-critical flow, form unwanted abrasion patterns around the vanes, the vanes themselves being damaged due to the high concentration of sediment load that passes through SBTs, and the vanes may impede access to an SBT.

As can be seen in the conceptual sketch of Figure 4, taken from the Solis physical model report (Solis 2010), it was observed that sediment bedload went from being spread out across the invert to being concentrated against the inner wall of the curve. Flow in SBTs can be considered stratified, with bedload sediment on the bottom, suspended particles in the middle or closer to the bed, and less sediment near the top of flow. The strong secondary current disturbs this stratification and pushes the less sediment laden flow down the outer wall of the bend then back

towards the inner wall. This current creates a flushing action that pushes bedload away from the outer wall.

The most current abrasion equation from Demiral (2020), and previous abrasion-rate equations utilize a unit gravimetric sediment supply rate (q_s) in units of [kg/(m·s)]. This parameter is the sediment load in kilograms per second divided by the width of the SBT invert. This parameter assumes that the sediment load is evenly distributed across the invert. However, when strong secondary currents due to bends in the SBT push the bedload to the inner curve, the unit rate of bedload can be significantly increased when the distribution of bedload transitions from nearly the full width of invert to just a fraction of the invert's width, as conceptually sketched in both Figure 4 and Figure *5*. The concentration of bedload, locally at and downstream of SBT bends, increases the abrasion rate. For instance, for a 4.0-meter-wide tunnel invert, if the bedload were concentrated to 1.0 m along the inside of a bend, the abrasion rate would be increased by a factor of 4.0 m/1.0 m or four times the abrasion rate in the tunnel when the bedload is evenly distributed across the invert.

The equation from Demiral (2020) for estimation of the abrasion rate in SBTs is given below:

$$A_r = \frac{Y_M}{k_v f_{st}^2} k_H P_S \frac{W_{im}^2}{L_p} q_s \qquad \text{(Eq. 2)}$$

Where:

A_r = vertical abrasion rate [m/s]

Y_M = Young's (elasticity) modulus [Pa]

f_{st} = splitting tensile strength or indirect tensile strength [Pa]

k_v = non-dimensional rock resistance or hydro-abrasion coefficient

W_{im} = mean vertical particle impact velocity [m/s]

L_p = particle hop length in [m]

q_s = unit gravimetric sediment supply rate [kg/(m·s)]

k_H = hardness coefficient $(MH/MH_B)^{1.3}$

P_S = Probability of Saltation = $1\text{-}1.05(T^*)^{-0.9}$ for hydraulicly rough beds

MH = Mohs hardness of abrasive particles

MH_B = Mohs hardness of bed lining material

The Demiral equation does not readily predict that abrasion is greatest along the inside of an SBT bend. Although there is a parameter which can be changed to reflect the reduction in bottom width, this parameter alone does not account for the increased abrasion rate. An additional adjustment may be needed for the probability of saltation, as particles moved into the zone of the inside bend may experience a higher probability of uplifting from the secondary current or be more prone to saltate due to increase in interparticle collisions. However, this concern is not the objective of this thesis, but the concern could use further study.

Although terms such as hop length, vertical particle impact velocity, or the cover effect term may also be impacted by the concentration of bedload to the inside bend, modification of the q_s term appears to be the most direct way to account for influence of the secondary current.

The design criteria guidance developed by Ippen and Knapp (1951) suggests that invert banking is also an effective treatment to reduce the surface oscillations in the flow. Invert banking may also consequently reduce the strength of the secondary current, which could also then reduce the unit concentration of sediment toward the inside of the curve.

From the USACE (1991) in EM 1110-2-1601,

$$\Delta y = C\frac{V^2 W}{gr} \qquad \text{(Eq. 3)}$$

Where:

Δy = rise in water surface between a theoretical level water surface at the centerline and outside water-surface elevation (superelevation)

C = coefficient (1 for rapid flow, rectangular cross-section, simple circular curves).

V = mean channel velocity

W = channel width at elevation of the center-line water surface

g = acceleration of gravity

r = radius of channel center-line curvature

However, instead of utilizing invert banking to reduce surface oscillations in the flow, this thesis considered invert banking along a bend to distribute bedload sediment more evenly across the invert as it passes around an SBT bend and thereby mitigate invert abrasion. This banking would be in the opposite direction as suggested by Knapp 1951. The purpose of SBT-bend invert banking would be to keep sediment more evenly distributed across the invert throughout a bend. The critical shields parameter, the transverse shear stress, and particle behavior output from the CFD-DEM model were evaluated to determine what amount of banking succeeded at a better distribution of sediment. These channel banking transverse slopes evaluated with CFD-DEM modeling are described in Section 3.6.

The Shields formula (Shields 1936) to determine the stability of granular material in flow, predicts that a particle is set to motion if the hydrodynamic forces are slightly higher than the retarding forces. This critical condition is expressed by the Shields parameter θ:

$$\theta = \frac{\tau}{(\rho_s - \rho)gd} \quad \text{(Eq. 4)}$$

Where:

θ = shields parameter (dimensionless)

g = gravitational constant (m/s^2)

τ = bed shear stress (Pa) = $\rho * g * h * S$

h = depth of flow (m)

S = energy slope or bed slope

d = particle diameter (m)

ρ_s = density of sediment particles (kg/m^3)

ρ = density of water (kg/m^3)

The critical Shield's parameter for incipient motion of a particle, θ_c, can be calculated using the critical shear stress, τ_c. The Shield's parameter will be utilized in Chapter 4 to analyze the CFD-DEM results.

CHAPTER 3. NUMERICAL-MODELING APPROACH

3.1 Overview

There are many limitations of the CFD-DEM modeling of sediment that passes through the Solis tunnel. Variables that can influence modeling results include the mesh cell size, temporal and spatial schemes, the sizes of sediment, the shape of sediment, the discharges, the number of particles, and the time step required to accurately simulate the interparticle and particle-bed collisions. This chapter discusses the decisions that went into choosing inputs for the modeling.

3.2 Computation Fluid Dynamic Model Selection

OpenFOAM software and the *interFoam* multiphase (*multiphaseInterFoam*) solver were used to simulate the alternatives with the RNG (Renormalization Group) k–ε turbulence closure model and the volume-of-fluid method for incompressible flows. As per Kadia (2024), the RNG k–ε turbulence closure model, with 1st-order spatial and temporal schemes replicated surface first wave extrema and found that the flow depths deviate marginally (within ± 2.1%), and that for the k–ε turbulence model, wave extrema downstream of the first deviated noticeably from the observed physical model data. Therefore, the RNG model was recommended for this study. The approach taken for this study used the RNG k–ε turbulence closure model, with 1st order spatial and temporal schemes replicated surface first wave extrema.

The *multiphaseInterFoam* solver was coupled with a DEM using LIGGGHTS, which stands for LAMMPS *improved for general granular and granular heat transfer simulations*. The CFD model was run to convergence, where the parameters such as depth and velocity remained constant throughout the domain. Then a CFD-DEM coupling model was initiated, which runs a DEM and CFD model at the same time, tracking the particles as they move through the flow

domain. The DEM model used was LIGGGHTS, which is a powerful discrete element modeling technique for optimization and design of particle processes (Hager 2018). In this study, the particle process is abrasion, and the optimization is the transverse tunnel slope that distributes the abrasion most evenly across the invert of the tunnel. The version of CFD-DEM coupling with *LIGGGHTS* used in this study was developed with the concepts in Vangoe (2017). The CFD-DEM coupling is unresolved, which means the flow around each individual particle is not resolved and must be modeled with particle property inputs like a radius, a drag coefficient, and an assumed shape (spherical). Typically, particles are small compared to the spatial resolution of the CFD mesh, which drastically reduces the computational time compared to resolved CFD-DEM at the cost of losing access to small-scale flow structures (Vangoe 2017). The CFD-DEM model is 4-way coupled, meaning (Traoré 2015) that –

- Fluid motion affects particle motion.
- In turn, particles affect the fluid flow (changing roughness of boundary).
- Particle motion can affect the motion of other particles.
- Particle motion is affected by channel walls.

The mesh was generated with *blockMesh*, such that the mesh changes uniformly with hexahedral cells along the SBT curvature (as can be seen in Figure 13), as opposed to producing a mesh with *snappyHexMesh*, which can create non-hexahedral cells. The *blockMeshing* of the SBT bend was achieved using the arc feature.

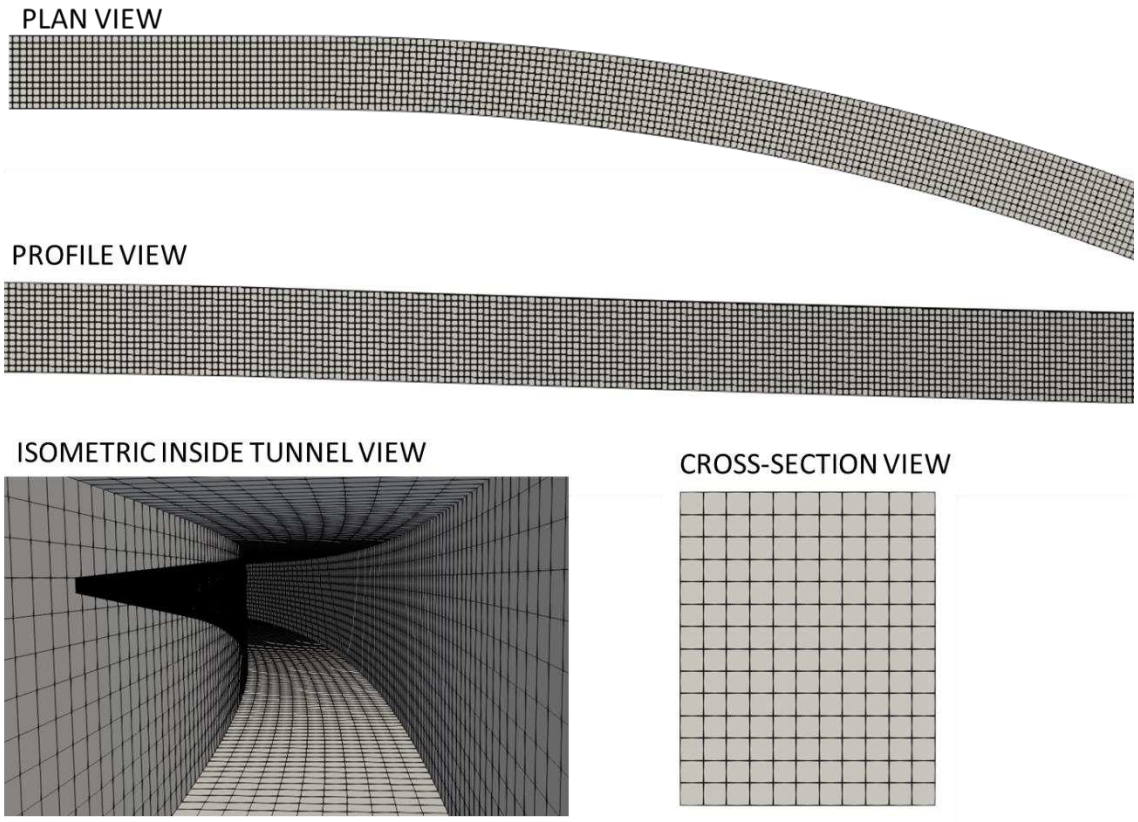

Figure 13. Zoomed in views of tunnel bend - mesh remains uniformly distributed around tunnel bend. A detailed model sketch with dimensions can be seen in Figure 14.

3.3 Model Plan

The Solis SBT channel bend was selected for testing different options for invert-banking (transverse slope), because this SBT has been extensively studied with physical modeling and has been operational since 2012. Additionally, this SBT demonstrated the impact of the secondary current's influence on abrasion of the SBT liner. The liner is formed from standard concrete, and in the CFD model was given a roughness height value of $k_s = 3$ mm (Müller-Hagmann, 2017). To reduce the amount of model runs required, only three discharges were run in the model, 102.16 m^3/s, 158.91 m^3/s and 215.67 m^3/s. These were the same flows used in the

physical modeling and CFD modeling in Kadia (2024) and coincide with flows used to design the SBT.

Dimensions for the Solis SBT were taken from Kadia (2024), in which wave extrema were analyzed in a physical model of length scale 1:22 (model/prototype) and replicated with numerical methods and an OpenFOAM CFD model. The CFD model was built in accordance with prototype scale. The radius of curvature in the SBT bend is 6.59 m, at model scale, or 145.00 m at prototype scale. The SBT has a 0.2 m-wide invert at model scale (4.4 m-wide invert at prototype scale). The SBT alignment has a 46.5° angle of deviation (amount of angle that SBT deviates from straight path). To mimic the physical model set up, the channel walls in the CFD model were set to be 5.0 m high, even though in actual SBT starts to transition to a semi-circular top once it reaches a vertical height of 2.48 m. The SBT's walls were left vertical to make numerical meshing easier, and to simplify the analysis. As referenced in Demiral (2020), the slope of the Solis SBT is 1.9%, and this slope was used in the model analysis. The downstream extent of the model, after the bend curvature continued downstream was 84.8 m; and the upstream extent was 200 m upstream bend. A full schematic of the model in plan view can be seen in Figure 14.

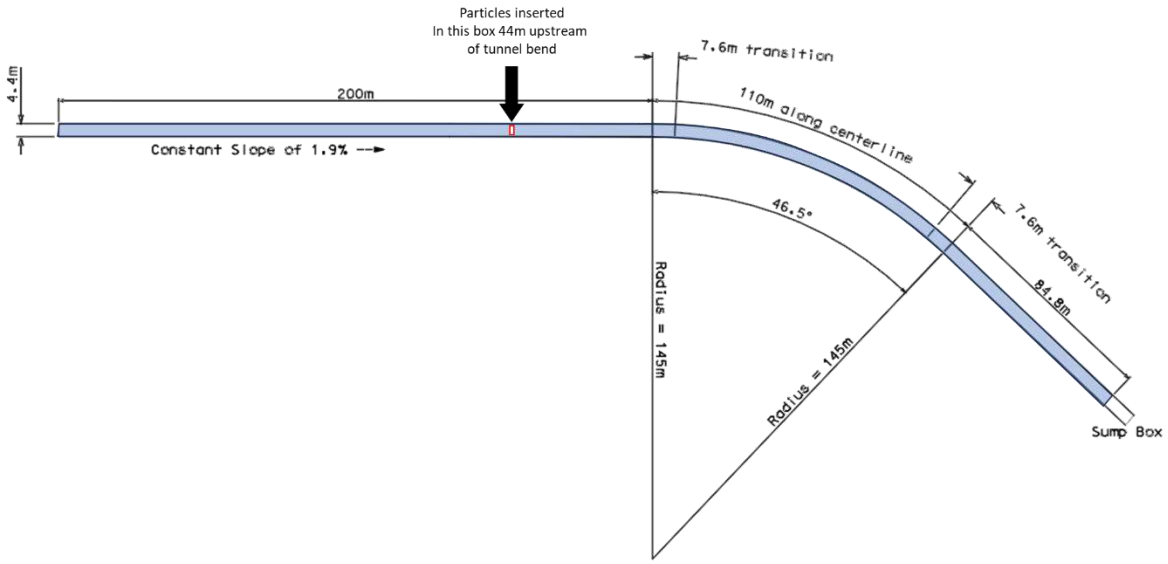

Figure 14. Schematic of model set up for modeling alternatives

Particles were inserted into the CFD model using a random number generator distribution template. The particles were placed in the domain at a starting speed of 1 m/s in the direction of flow 44.0 m upstream of the start of the tunnel bend to allow a distance that enables the particles to distribute evenly across the invert of the channel before entering the tunnel bend. Each alternative used the same random number generating seed so that they all started with the exact same particle distribution. Particle attribute inputs into the DEM model included a drag coefficient of 0.5, a coefficient of restitution of 0.9, Young's Modulus Elasticity (Y_M) set to $4x10^6$ Pa, and a density of 2650 kg/m^3. Sensitivity to these parameters appeared to be negligible in terms of the behavior of the particles moving to the inside bend. The real-world particles or sediment load have a much higher Y_M value, but the timestep must also be decreased significantly to accurately capture the interparticle and wall-particle interactions, which significantly increases the model run times. If the Y_M value was increased too much, particles started to behave more erratic and would often transport through the walls of the tunnel. A default value of $Y_M = 4x10^6$ was selected as a balance between a high and low values.

3.4 Discharge Alternatives

Three flows were evaluated in the physical model Kadia (2024). Dimensional analysis was applied to scale these discharges using Froude similitude, ensuring dynamic similarity of discharge between the model and prototype (where Q is proportional to $L^{5/2}$) and these discharges are shown in Table 1. The sediment was scaled geometrically from the physical model. The flows are moving on a fixed bed, and not a loose bed, so the Froude similitude and geometric scaling is valid.

Table 1. Flows converted from Solis physical model to prototype discharges (Kadia 2024).

Value in the Physical Model		**Prototype Value**	
Q (m^3/s)	**H** (m)	**Q** (m^3/s)	**h** (m)
0.045	0.109	102.16	2.40
0.07	0.151	158.91	3.32
0.095	0.175	215.67	3.85

3.5 Mesh Dependency

A mesh-dependency analysis was conducted to determine how sensitive the results of the simulation were to different mesh sizes. It was determined through this analysis that further refinement of the mesh may be warranted to depict velocities, depths, and shear stresses more accurately in the simulation. However, this study is focused on a comparative analysis to determine what transverse slope configurations distribute sediment most evenly along the invert of the tunnel. The unresolved CFD-DEM method cannot be applied for cases where the particle size is greater than the CFD cell size, the cell must be larger the sediment sizes being evaluated. This restricts the resolved flow fields to a relatively coarser scale (Jaiswal et al. 2023). In other

words, the mesh size cannot be smaller than the particle size. The largest particle size in the simulation was 0.4 m, which was the maximum evaluated because for the tunnel conditions; moreover as Figure 15 shows, it was the largest particle size on the threshold between saltation and bedload as per Raudkivi (1998).

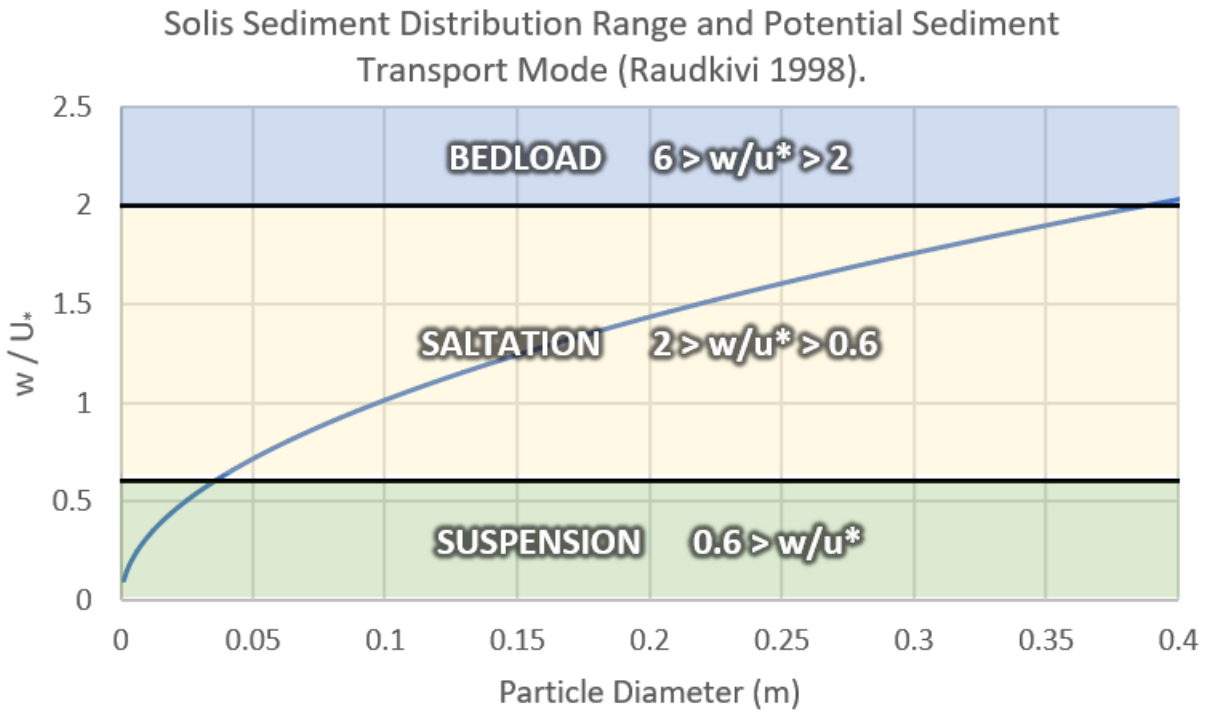

Figure 15. Potential for bedload, saltation or suspension transport modes based on particle diameter; values calculated using normal depth equation for Solis Tunnel with 158.9 m^3/s; where w = fall velocity, and U_* = shear velocity.

It was determined in the study that the larger mesh size of 0.4 m was adequate to represent the physical phenomena of secondary currents and the resulting transverse shear stress, despite outputs from smaller mesh sizes indicating that mesh convergence had not been reached. A verification CFD-DEM simulation demonstrated similar results to what was found in Kadia 2024; finding that particle sizes between 0.08 m and 0.26 m in diameter, with a 2400 kg/m^3

density, all traveled to the inside bend (see Figure 16). The CFD-DEM verification model was in close agreement with the photographs taken in Kadia (2024).

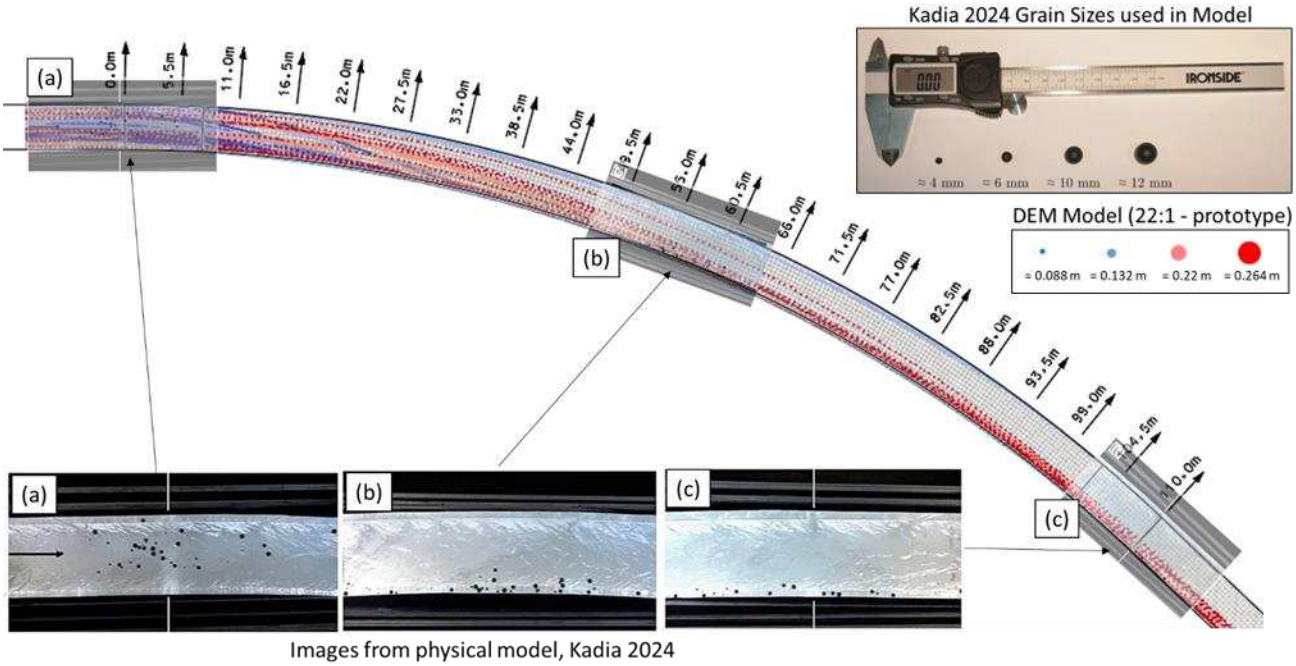

Figure 16. Comparison of CFD-DEM modeling with 158.9 m3/s flow, 0.4 m mesh resolution with 0.043 m, 0.067 m, 0.111 m and 0.133 m diameter particles (particle density was 2400 kg/m^3). Like the physical model, ten of each particle size were inserted into the flow: (a) beginning of curve; (b) mid-point of curve or bend: and (c) end of curve or bend.

A faster computational time was more desirable than accuracy of the simulation, as the computation times for the CFD-DEM model were considerably long when running all model alternatives, including additional computation time for the DEM model, and additional time needed for the DEM model particle resident time for slower moving particles to run through the length of the tunnel. The Froude number remained around 2 for flows in all simulations and only saw a few tenths of a reduction for the smallest mesh case. Results for the stand alone CFD model mesh convergence analysis (no DEM modeling incorporated), including run times,

average velocities, cell sizes, superelevation (Δy), and Froude number can be seen in Figure 17 and Table 2.

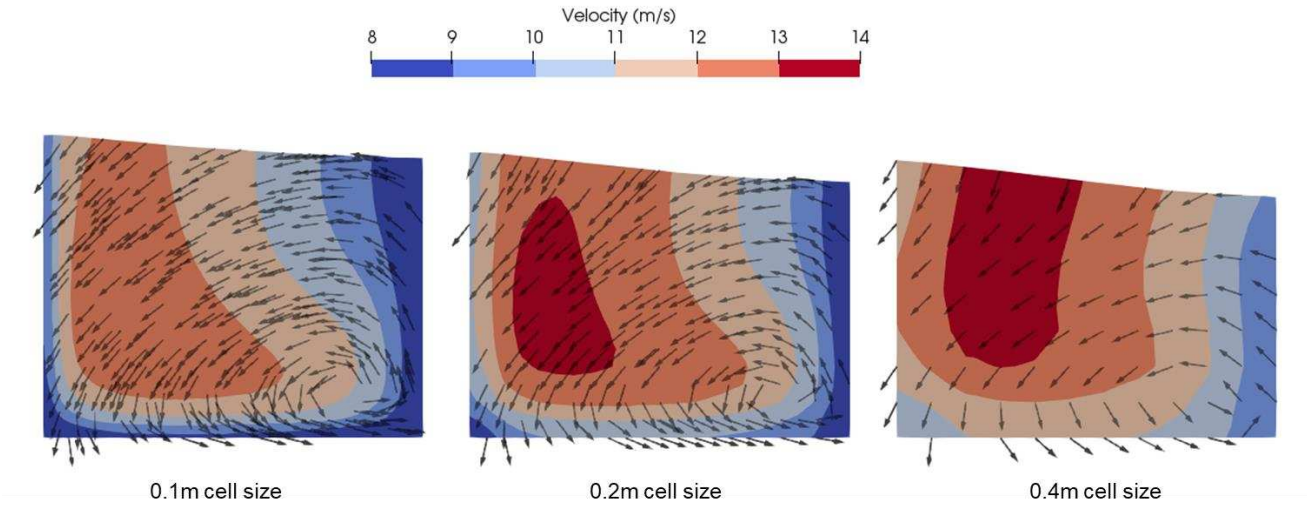

Figure 17. Mesh convergence immediately downstream of the Solis SBT bend. (Cell size indicated)

Table 2. Convergence results for 3 different mesh cell sizes: 0.4 m, 0.2 m, and 0.1 m.

Cell Size (m)	**Compute Time***		**Average Velocity** (m/s)	**Δy** (m)	**Average Depth** (m)	**Froude No.**	**No. of Cells**
	(seconds)	(hours)					
0.4	680	0.2	11.9	0.422	3.002	2.200	146,608
0.2	16,719	4.6	11.6	0.338	3.135	2.092	1,172,864
0.1	285,705	79.4	11.0	0.265	3.377	1.906	9,382,912
0.05**	N/A	N/A	N/A	N/A	N/A	N/A	75,063,296

*Compute times are for CFD model run only, not CFD-DEM coupled model.
**Although not computed, the number of cells reported to show significance of halving cell size

The streamwise average velocity was compared to the transverse velocities along the bottom 0.4 m of the SBT for the 0.4-m, 0.2-m and 0.1-m mesh sizes. As can be seen in Figure 18, the mesh begins to converge on the percent of streamwise flow in the transverse direction beyond decreasing mesh size of 0.2 m. The largest mesh size (0.4 m) and smallest mesh size (0.1 m) had a maximum streamwise to transverse velocity percentage of 5% and 7% respectively. It is

important to note that this analysis utilizes the larger mesh size of 0.4 m to reduce computational demand and run times. However, this arrangement may underpredict the percentage ratio of streamwise to transverse velocity by as much as 28.5% ([100% – 5%/7%] = 28.5%).

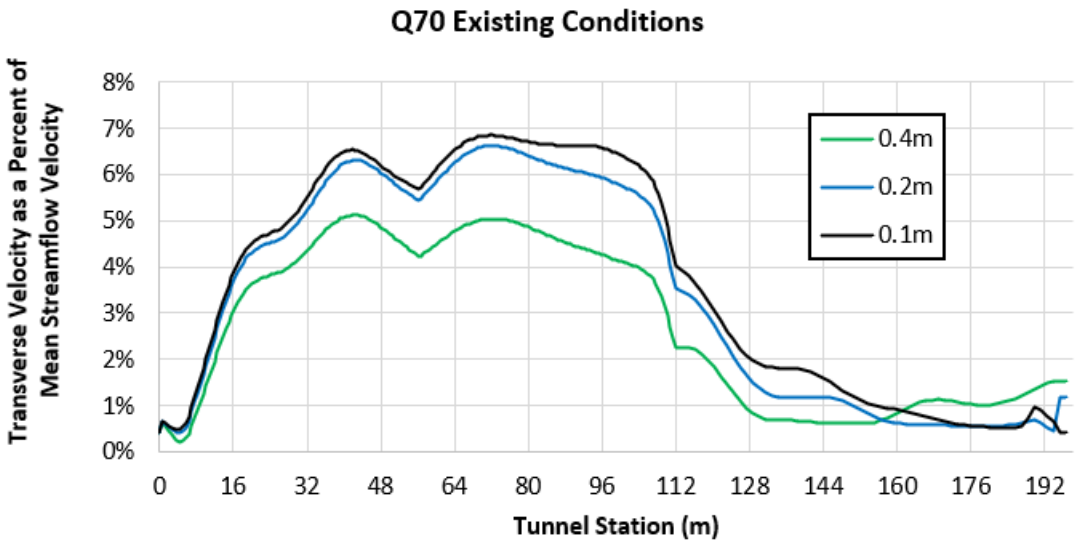

Figure 18. Comparison of transverse velocities along bottom 0.4 m of the SBT between mesh sizes of 0.4 m, 0.2 m and 0.1 m. Station 0 is the beginning of the invert's curvature, or an SBT bend.

The mesh size will also influence the shear stress parameter output from CFD, with a finer mesh giving a more accurate answer. The shear-stress symmetric tensor (R) can be calculated more accurately with finer near wall mesh resolution. *OpenFOAM*'s wallShearStress function computes wall shear stress with the below equation (*OpenFOAM* 2019):

$$\tau = \mathrm{R} \cdot \mathrm{n} \qquad \text{(Eq. 5)}$$

Where:

τ = Wall shear stress vector (m^2/s)

R = Shear-stress symmetric tensor (retrieved from turbulence model)

n = Patch normal vector (into the domain)

To get a final shear-stress value in SI units, the output from *OpenFOAM* is multiplied by the density of water, ρ = 1000 kg/m^3, to give the shear stress units of N/m^2.

3.6 Channel Banking Alternatives

All alternatives of invert banking transitioned from an invert that had 0% transverse slope to the invert-banking alternative via a transition of 7.6 m in the streamwise direction. The ramp-up slope could have been held constant, but either scenario, holding the slope constant, or the distance constant, may influence the behavior of the sediment. For instance, a constant upstream transverse slope for the 10% transverse slope alternative may push sediment over to the outer wall side of the tunnel before the sediment is influenced by the secondary current. Ramping the slope up for a length of over 7.6 m, for the 10% slope, may also push sediment to the outside bend. The concept of redistributing the bedload with the transverse slope is shown in Figure 19. The sketch of how the transverse slope transition was implemented in the model can be seen in Figure 20.

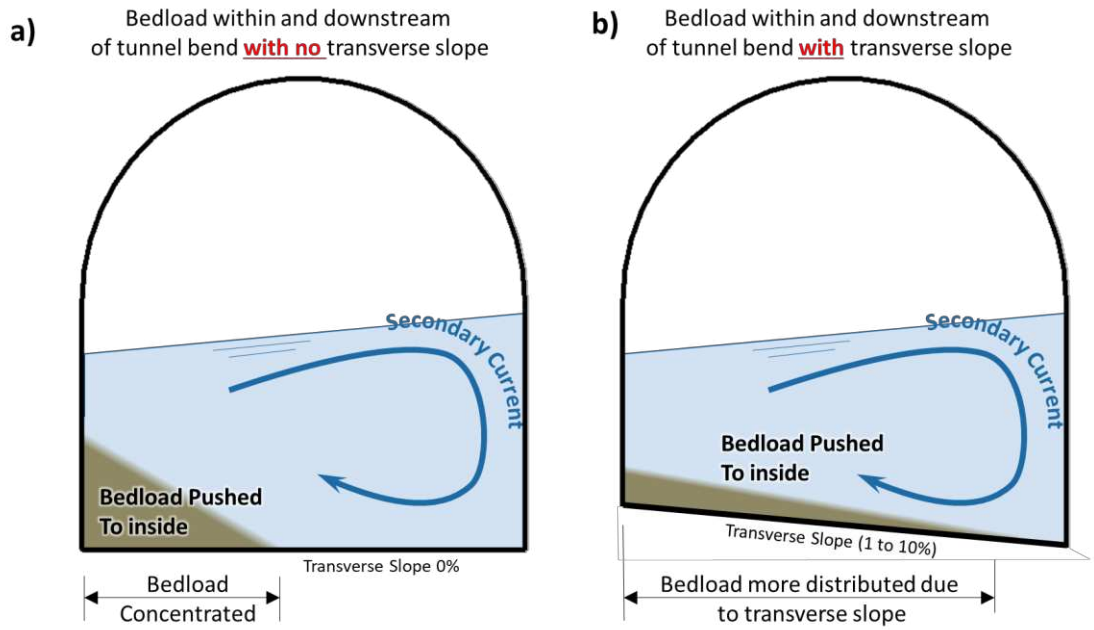

Figure 19. Sediment in an SBT bend: (a) conceptual sketch of sediment being concentrated to inside of tunnel bend; and (b) and transverse slope redistributing sediment along the SBT invert. (Cross-sections are looking upstream.)

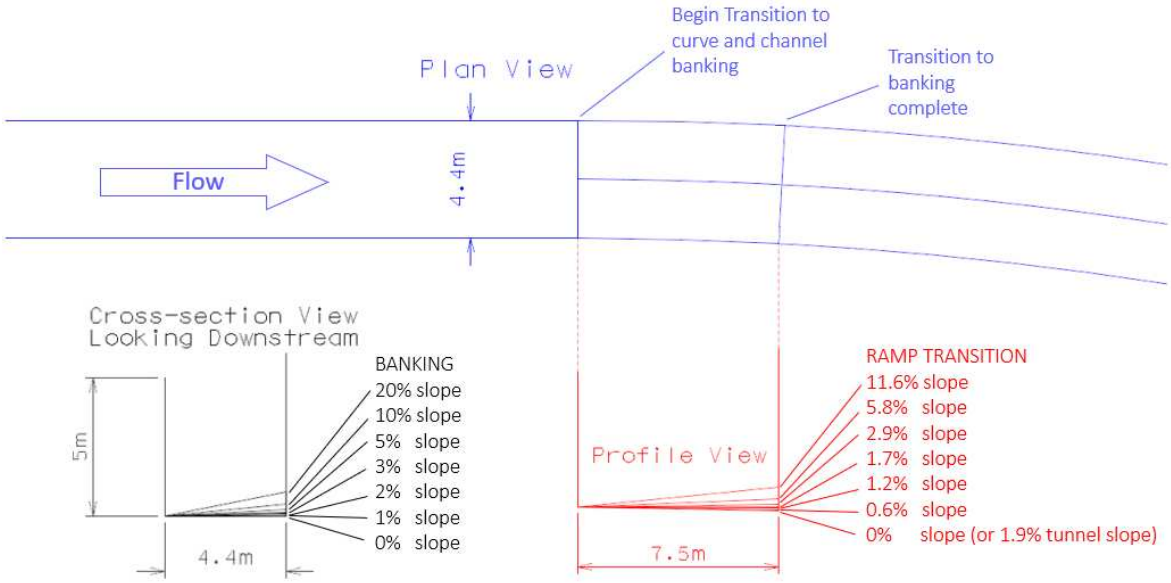

Figure 20. Conceptual sketch of channel banking alternatives and configuration within the model (Note: more configurations than what are shown here were assessed.)

Transverse slopes of 0%, 1%, 2%, 3%, 4%, 5%, 6%, 7%, 8%, 9% and 10% were evaluated in the CFD-DEM modeling to build a comprehensive picture of how the transverse sloping distributes a range of particle sizes across the tunnel invert. A 20% banking alternative was done only to demonstrate transverse shear-stress sensitivities to banking alternatives as discussed in Section 3.5, Mesh Dependency.

3.7 Sediment Size

As stated in the physical model report for the Solis SBT (Solis 2010): *"In the reservoir, the grain distribution is strongly influenced by sorting effects. In the area around the dam root, mainly coarse material remains. Fine particles are transported further towards the dam wall. The particle distribution in the area around the dam root is of interest in the project, as it characterizes the coarse bed load brought in by the Albula. To simulate the flowing bed load in*

the model, the grain distribution derived from the line sample at the dam root is used. The corresponding characteristic grain sizes are shown in... [Table 3]." Figure 21 shows the particle-diameter distribution used for the physical model.

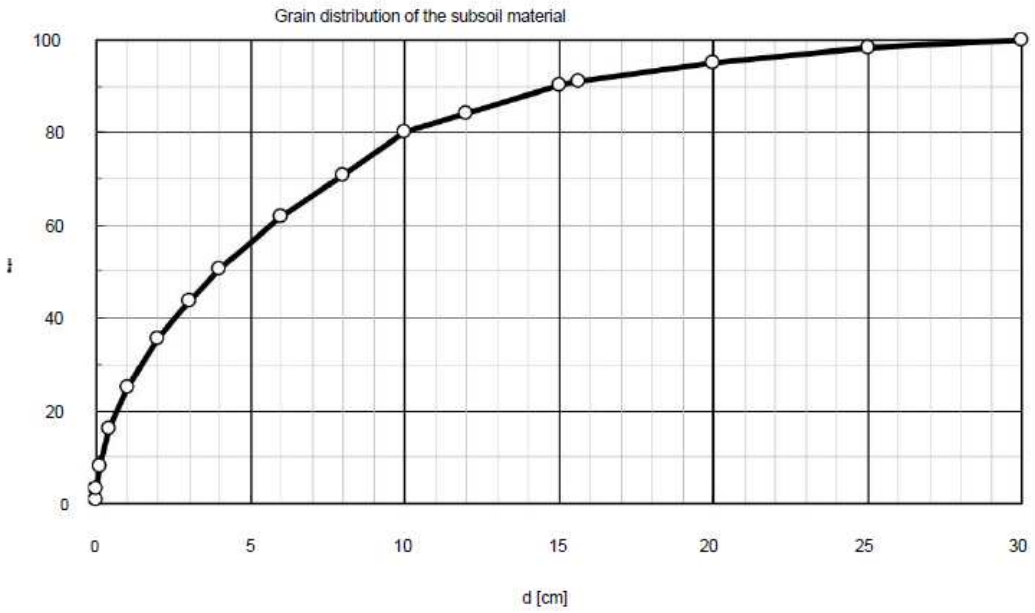

Figure 21. Particle diameter, d, distribution used in the physical model (Solis 2024).

Table 3. Characteristic particle size distribution for Solis SBT converted from line distribution (Solis Physical Model report).

Characteristic Grain size	Line sample
dm	6 cm
d50	4 cm
d90	15 cm

A range of particle sizes from 0.04 m to 0.4 m, also encompassing the size distribution of the physical model report (Solis 2010), was evaluated the CFD-DEM modeling. This particle size

range also encompassed the range of sizes that are predicted to be in saltation when flowing through the tunnel, as calculated using Raudkivi (1998) and shown in Figure 15.

3.8 Probability of Saltation

As already discussed in Section 3.5, a factor in selecting the mesh cell size was the particle sizes being evaluated. The most relevant particle sizes to evaluate are those that saltate in the tunnel and are also a large portion of the sediment grain size distribution. This section will cover why saltation is an important factor, and the methods of determining the probability of saltation. Flow can transport particles through the tunnel in the rolling, sliding, saltation, or suspension modes. Figure 22 shows these various transport modes. The rolling/sliding and the suspension modes are assumed to have a negligible effect on abrasion (Sklar and Dietrich, 2004). Therefore, a particle size which makes up the highest percentage of the grain distribution and has a high probability of saltation should be considered as the most important size that will cause abrasion and will be the primary focus during the evaluation of each transverse slope alternative. Figure *23* shows a compilation of data gathered from Auel et al., 2017a that shows the probability of rolling vs the excess transport stage.

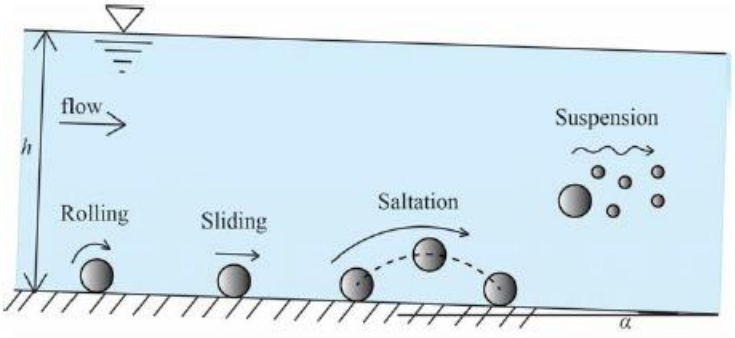

Figure 22. Sketch of various transport modes (Abbott and Francis 1977).

The probability of a particle rolling can be found with the equation (Auel et al 2017a):

$$P_R = 1.84(T^*)^{-0.94} \text{ for } 0 \leq P_R \leq 1 \qquad \text{(Eq. 6)}$$

Where P_R is the probability of rolling and T^* is the excess transport stage $(\theta/\theta_c - 1)$

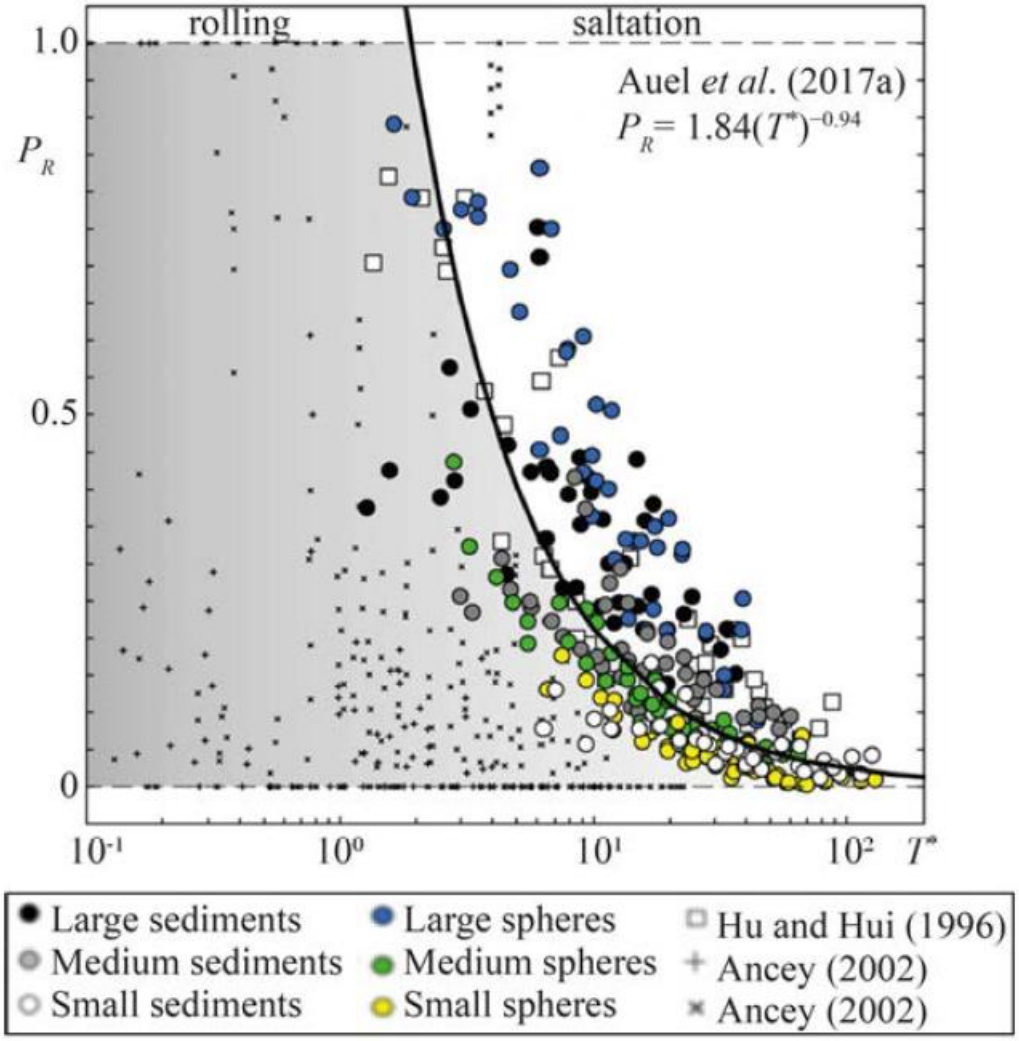

Figure 23. Rolling probability P_R versus the excess transport stage T* showing the literature.

data of Hu and Hui (1996a), Ancey et al. (2002) and Auel et al. (2017a) with a data-fitting curve

(adapted from Auel et al., 2017a)

From Sklar and Dietrich (2004) the excess transport stage can be defined as

$$T^* = \frac{\theta}{\theta_c} - 1 = \left(\frac{U_*}{U_{*C}}\right)^2 - 1 \qquad \text{(Eq. 7)}$$

Where friction velocity (U_*) or "shear velocity" in this equation is equal to

$$U_* = \sqrt{gR_hS_b} \qquad \text{(Eq. 8)}$$

Where:

$R_h = A_w/P_w$ = area divided by wetted perimeter = hydraulic radius of channel

S_b = channel bed slope

Abrasion experiments performed in Demiral (2020) found that the transition from hydraulically rough regime occurs at an early stage of abrasion. From Demiral (2020) the saltation probability (P_S) for a hydraulically rough beds, as found in SBTs, is:

$$P_S = 1 - P_R = 1 - 1.05(T^*)^{-0.9}, 0 \leq P_S \leq 1, \text{where } T^* > 1.05 \qquad \text{(Eq. 9)}$$

Compared to the saltation motion, the suspension mode covers larger trajectory lengths between two consecutive impacts (Müller-Hagmann, 2017). The transition from saltation to suspension mode occurs when the vertical components of turbulent velocity and particle settling velocity are equal (Francis and Bagnold, 1973) as described in the equation, the probability of suspension is:

$$P_{sus} = \frac{1}{16}\left(16 - \frac{V_s}{U_*} - \frac{V_s^2}{U_*^2}\right)\exp\left(\frac{V_s}{U_*}\right) \qquad \text{(Eq. 10)}$$

Where V_s is the particle settling velocity. For the given grain size distribution discussed in Section Sediment Size, the probabilities of suspension, saltation, and rolling computed with Eq 5, 8 and 9, and are shown in Figure 24 and Table 4.

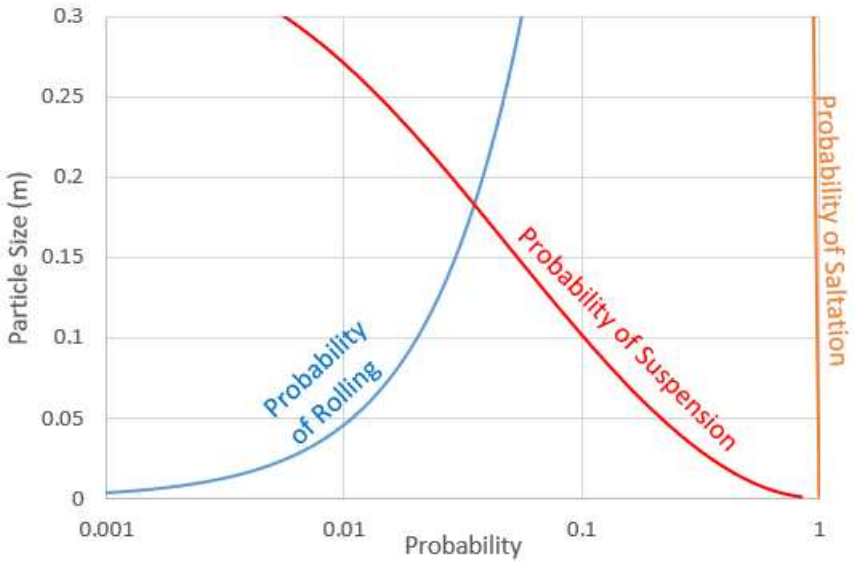

Figure 24. Rolling, suspension, and saltation probabilities for range of sediment sizes that pass-through the Solis SBT.

Table 4. Table format of probabilities of range of particle sizes that pass through the Solis SBT.

Particle Size (m)	Probabilities (% Chance)		
	Rolling	Saltation	Suspension
0.06	1.28%	98.72%	18.34%
0.1	2.04%	97.96%	10.28%
0.15	2.95%	97.05%	5.38%
0.2	3.84%	96.16%	2.84%
0.3	5.60%	94.40%	0.00%
1	18.02%	81.98%	0.00%

Although rolling, saltation and suspension equations strongly suggest that the range of particle sizes being evaluated in this study may be in saltation, the CFD-DEM model did not appear to accurately replicate the saltation physical phenomena. For the most part, particles remained near the bed of the invert for the entire simulation and did not hop or saltate. Introducing more particles into the flow did seem to produce saltation, but this appeared to be due to the interparticle collisions, and once particles were separated from others around them, they did not

saltate on the bed unless impacted by other particles. The lack of saltation could be due to the turbulence modeling used, mesh size, the sediment-particle input properties, the wall boundaries in the DEM model, the contact method which influences how the particles and invert of the tunnel interact, or a combination of all these factors and others not considered. The presence of the saltation in simulations with at least 1000 particles did not appear to influence whether they were impacted by the secondary current. Or, in other words, whether the particles saltated or not, they exhibited the same behavior of being moved to the inside bend by the secondary current.

CHAPTER 4. RESULTS

To evaluate the behavior of different particle sizes in the CFD-DEM model, the diameters 0.04 m 0.08 m, 0.12 m, 0.16 m, 0.2 m, 0.24 m, 0.28 m, 0.32 m, 0.36 m, and 0.40 m were inserted into the model for each of the discharges of 102.16 m^3/s, 158.9 m^3/s and 215.67 m^3/s. Transverse slope alternatives of 0%, 1%, 2%, 3%, 4%, 5%, 6%, 7%, 8%, 9%, and 10% were used. A total of 33 separate model simulations were conducted (11 different transverse slopes multiplied by 3 different flows). As described in Section 3.7, the particle diameters were selected based on the particle size distribution relevancy to the Solis SBT, and to the range of saltation potential calculated for the medium flow of 158.9 m^3/s.

Each simulation began with approximately 1000 particles (100 of each particle size) inserted 44 m upstream of the beginning of the bend. Particle impacts caused some of the smaller particles to leave the domain, likely through the walls of the SBT; in practice the particles would bounce off the wall and return to the flow. The loss of particles was likely due to the large forces and large timestep, and resulted in a particle count of typically between 950-960 at the end of a simulation.

Tracer paths were used to track each particle as they crossed through a slice placed at the midpoint of the curve and at the end of the curve as seen in Figure 25. This method effectively captured the particle trajectories in a single image as can be seen in Figure 26 through Figure 35, all of which show how the change in transverse slope changes the distribution of particles along the SBT's invert at the middle of the bend. The general vector of secondary current is also shown in these figures.

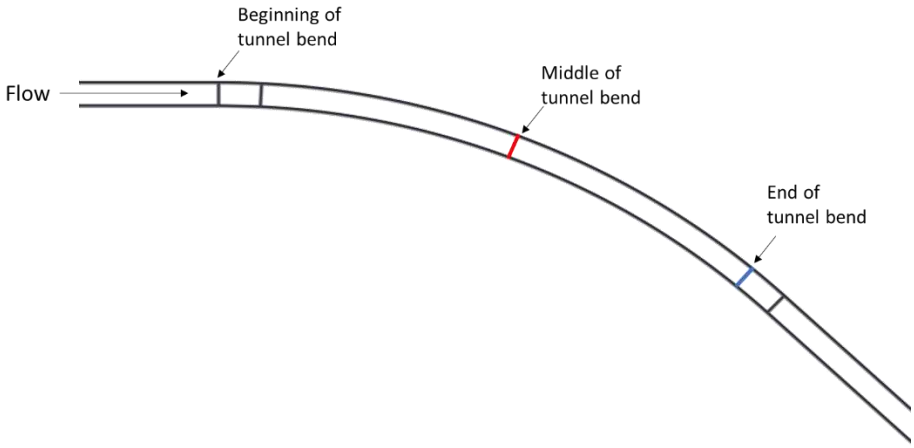

Figure 25. Location of slices used for data collection at beginning of tunnel, middle, and end of curve.

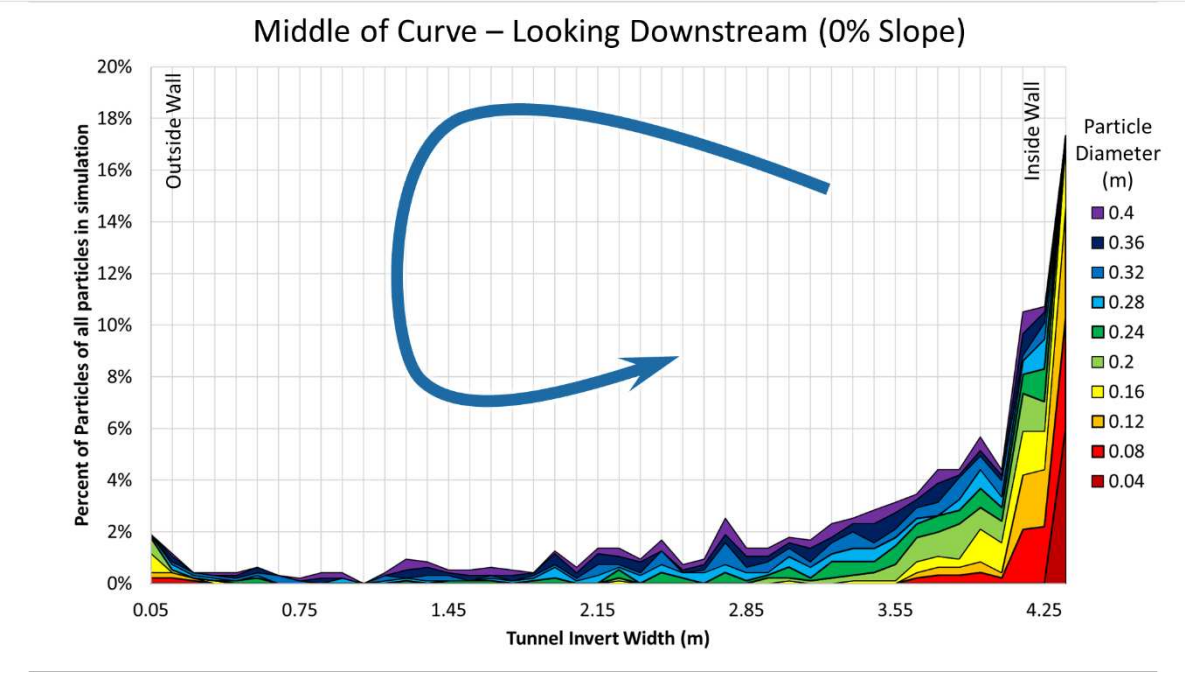

Figure 26. Particle distribution at Middle Curve slice for 158.9 m^3/s and 0% transverse slope.

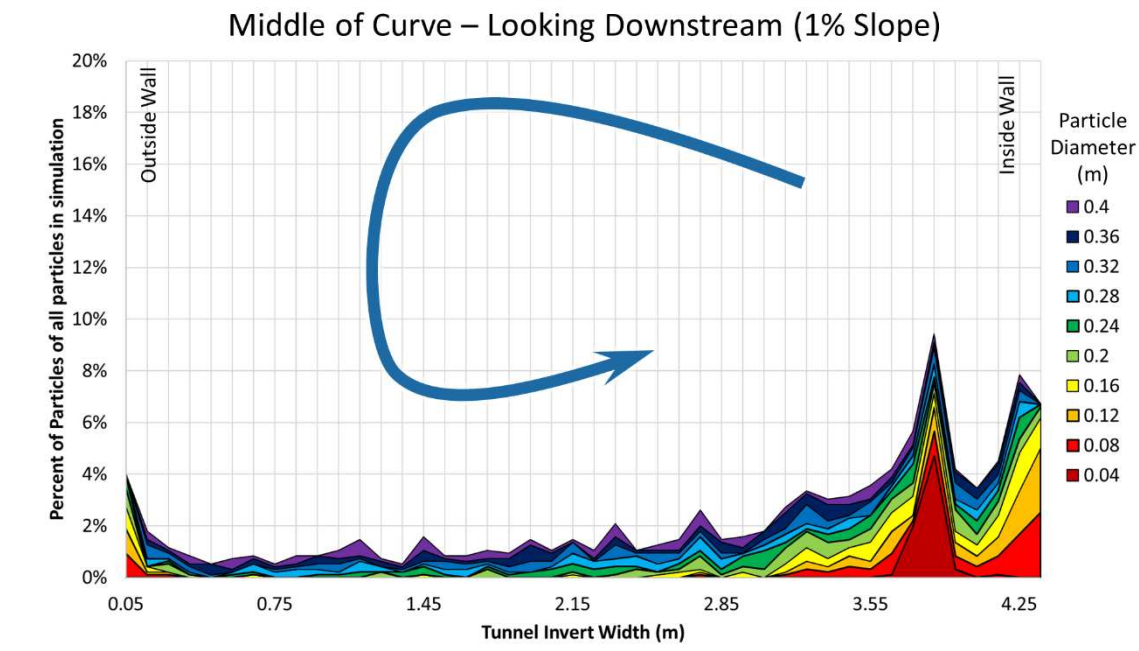

Figure 27. Particle distribution at Middle Curve slice for 158.9 m^3/s and 1% transverse slope.

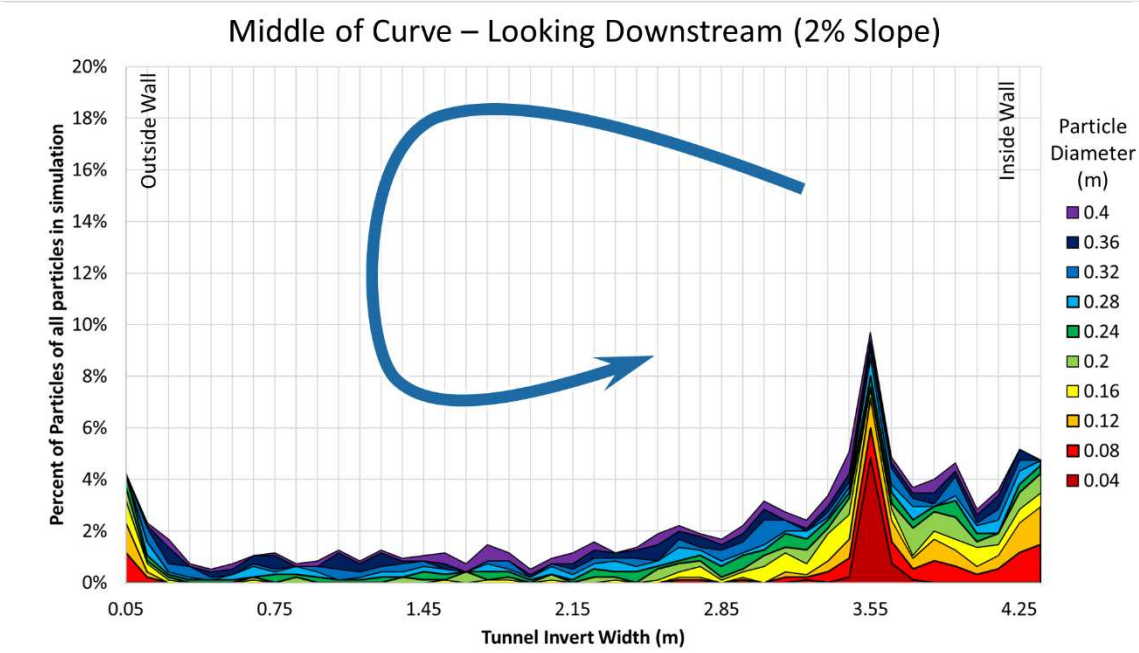

Figure 28. Particle distribution at Middle Curve slice for 158.9 m^3/s and 2% transverse slope.

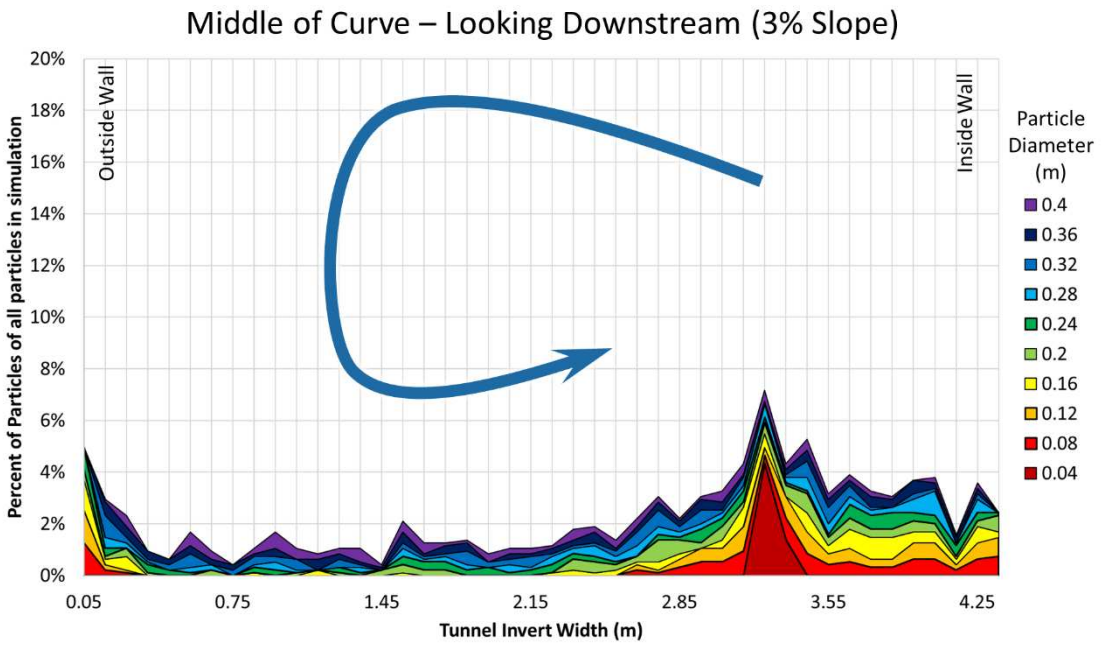

Figure 29. Particle distribution at Middle Curve slice for 158.9 m^3/s and 3% transverse slope.

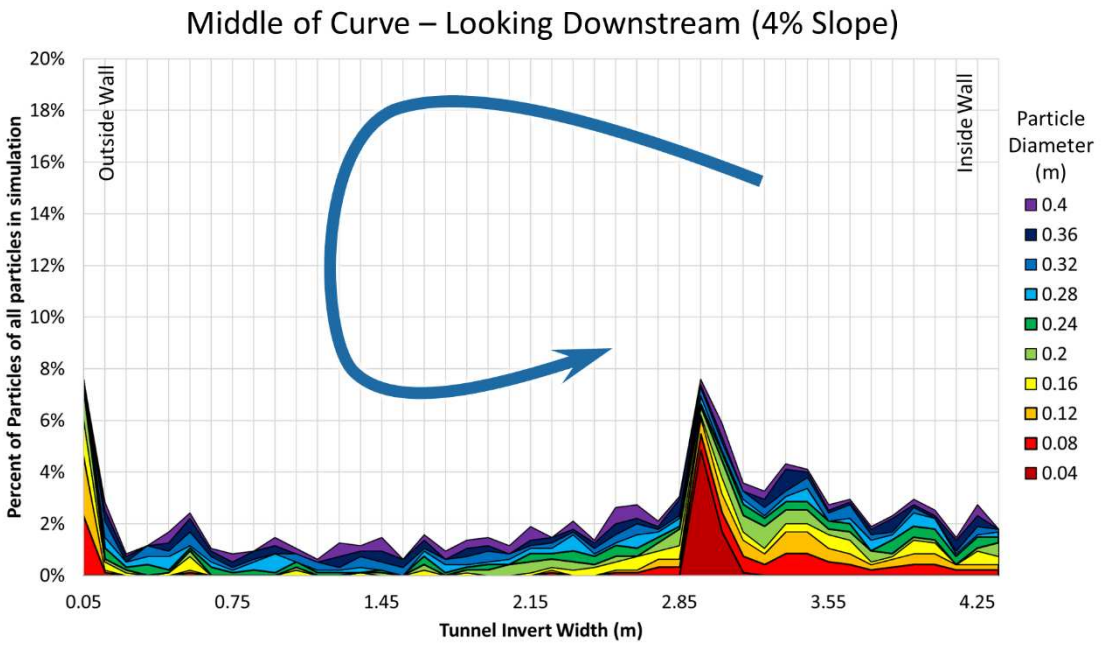

Figure 30. Particle distribution at Middle Curve slice for 158.9 m^3/s and 4% transverse slope.

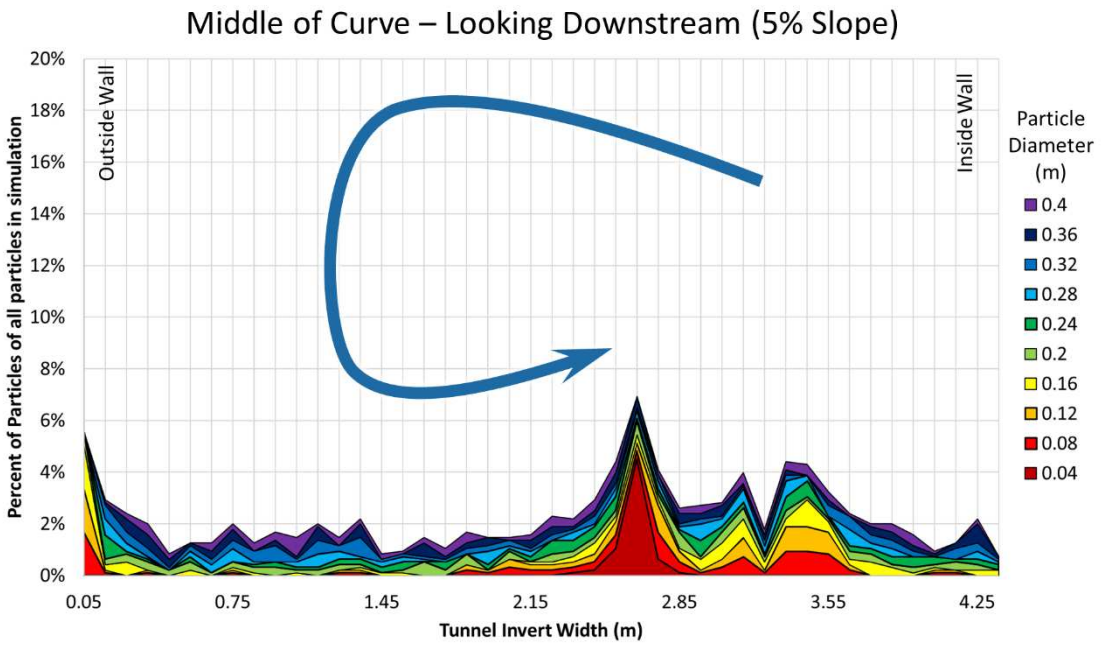

Figure 31. Particle distribution at Middle Curve slice for 158.9 m^3/s and 6% transverse slope.

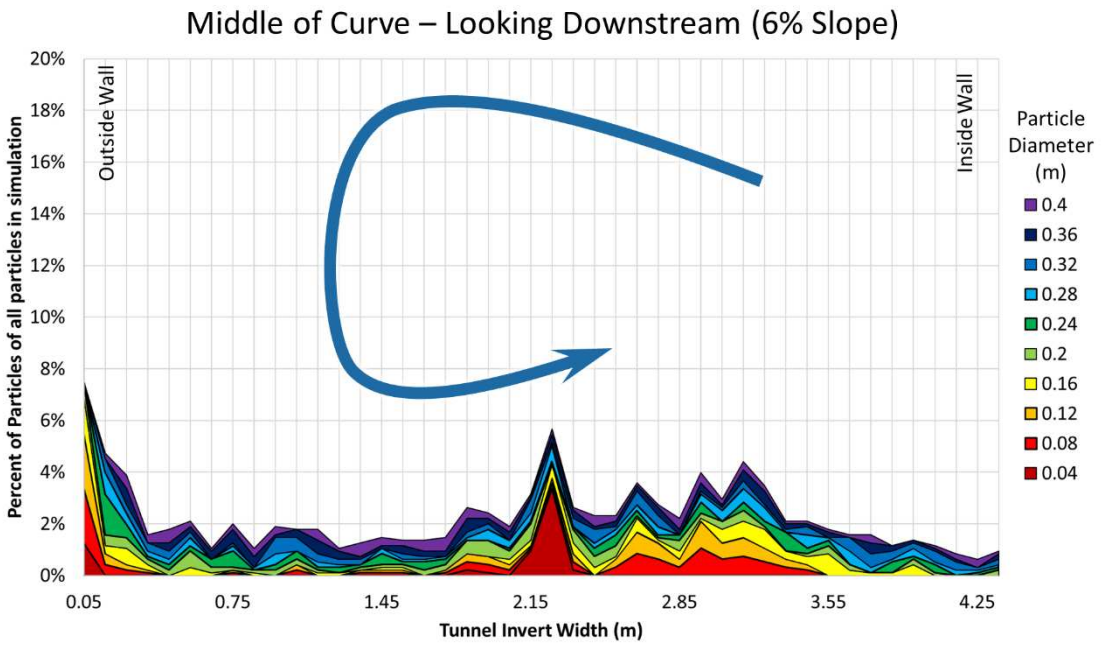

Figure 31. Particle distribution at Middle Curve slice for 158.9 m^3/s and 6% transverse slope.

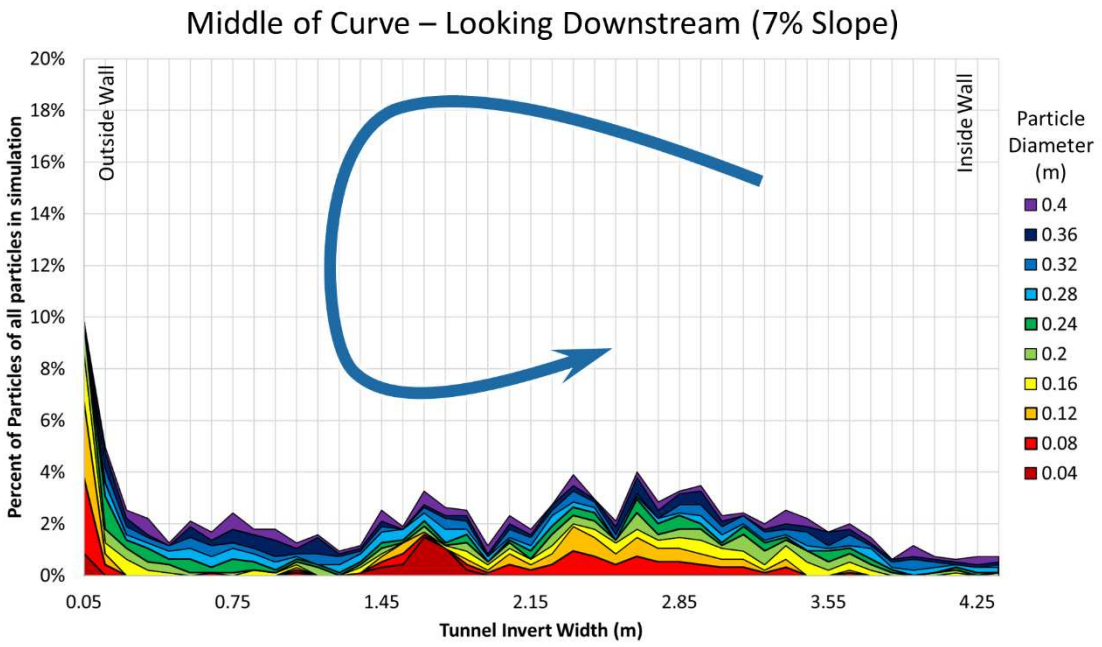

Figure 32. Particle distribution at Middle Curve slice for 158.9 m^3/s and 7% transverse slope.

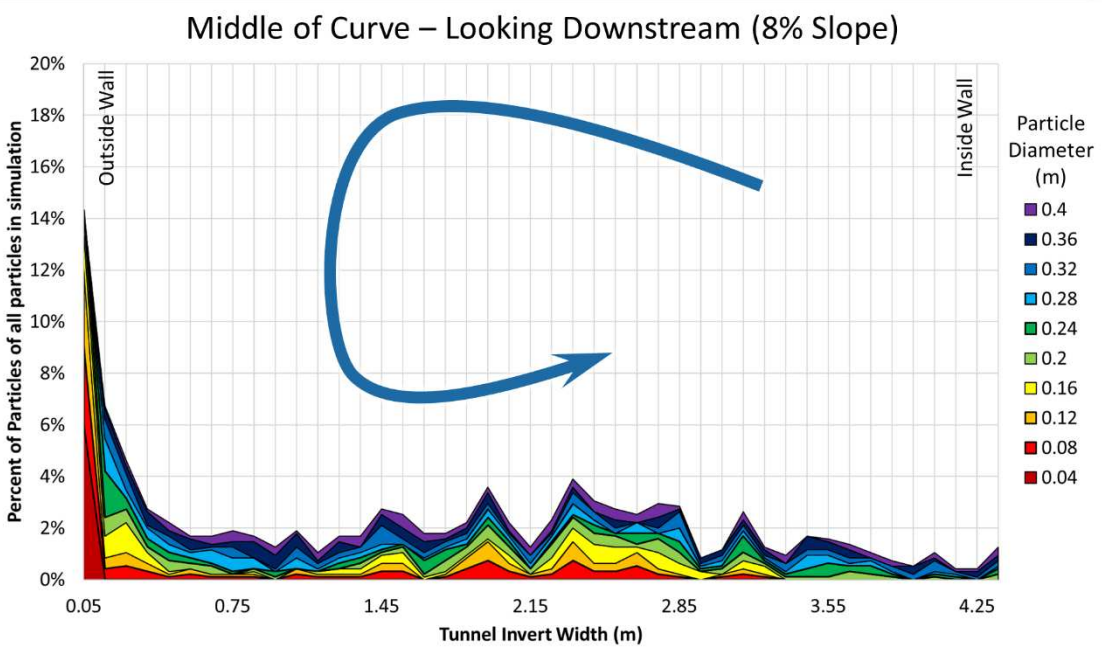

Figure 33. Particle distribution at Middle Curve slice for 158.9 m^3/s and 8% transverse slope.

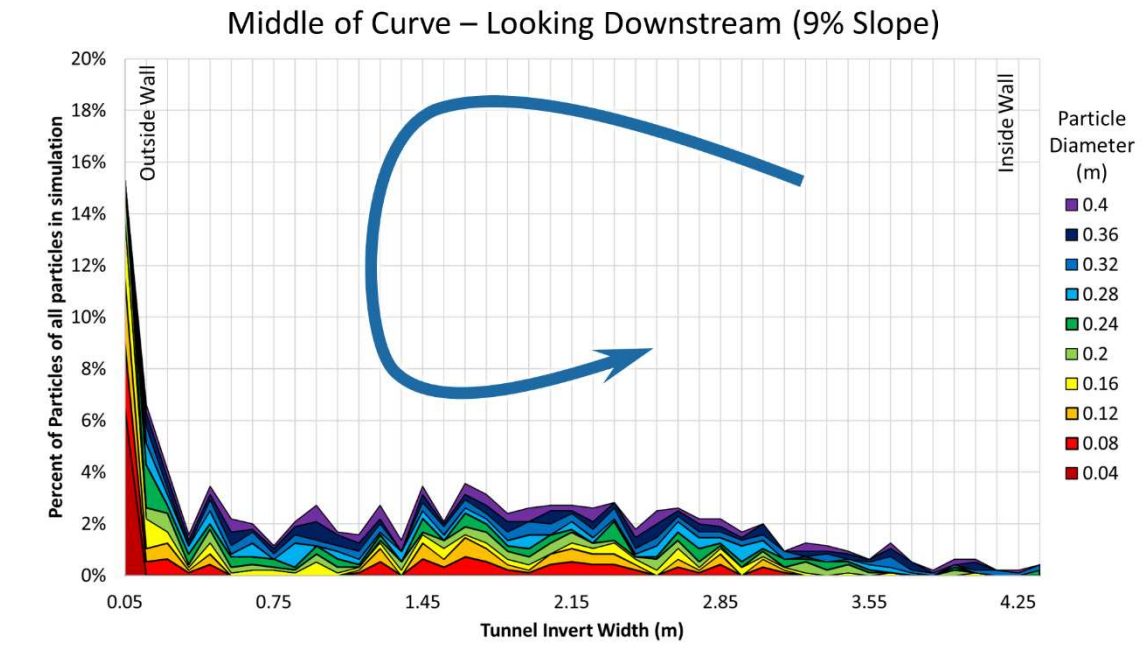

Figure 34. Particle distribution at Middle Curve slice for 158.9 m^3/s and 9% transverse slope.

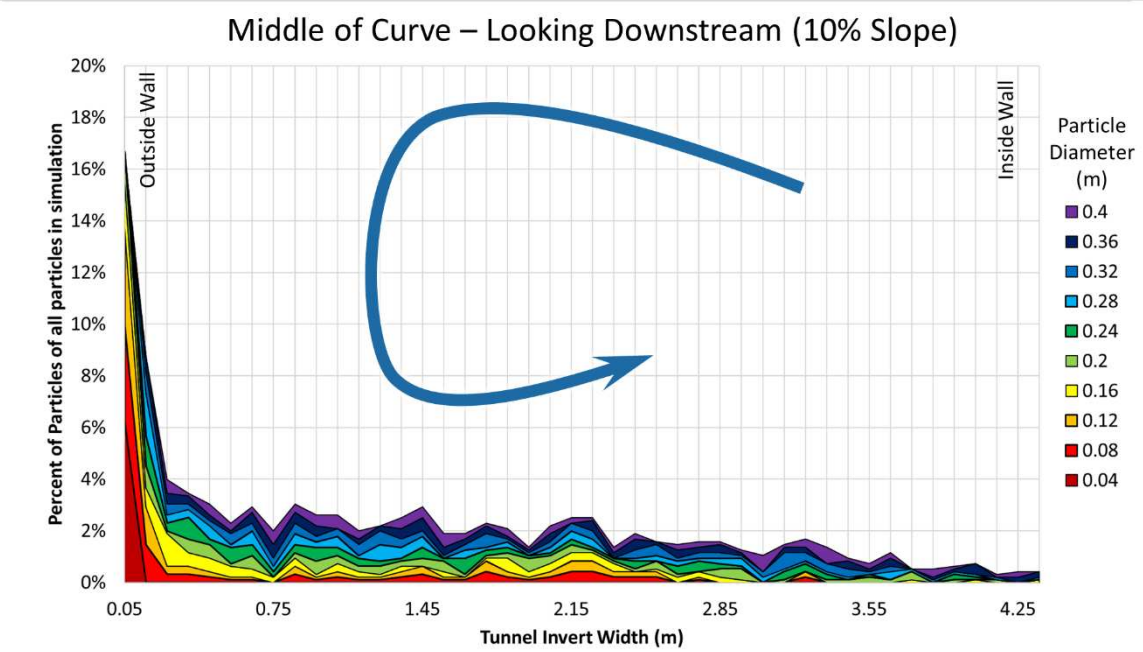

Figure 35. Particle distribution at Middle Curve slice for 158.9 m^3/s and 10% transverse slope.

The center of each particle distribution was computed and its distance from the center of the SBT is shown in Figure 36 and Figure 37 for the middle of curve and end of curve, respectively, and Q = 158.9 m^3/s. A distribution center value of 0 is closest to the center of the tunnel. The model predicts that smaller particles are more influenced by the primary flow aided by the secondary current and transverse sloping. Smaller particles either accumulated at the bend's inside bank with a 0% transverse slope, or they accumulated to the outside bank with a 10% slope. Larger particles are also influenced by the secondary current and transverse slope, but not to the same extent as are the smaller particles.

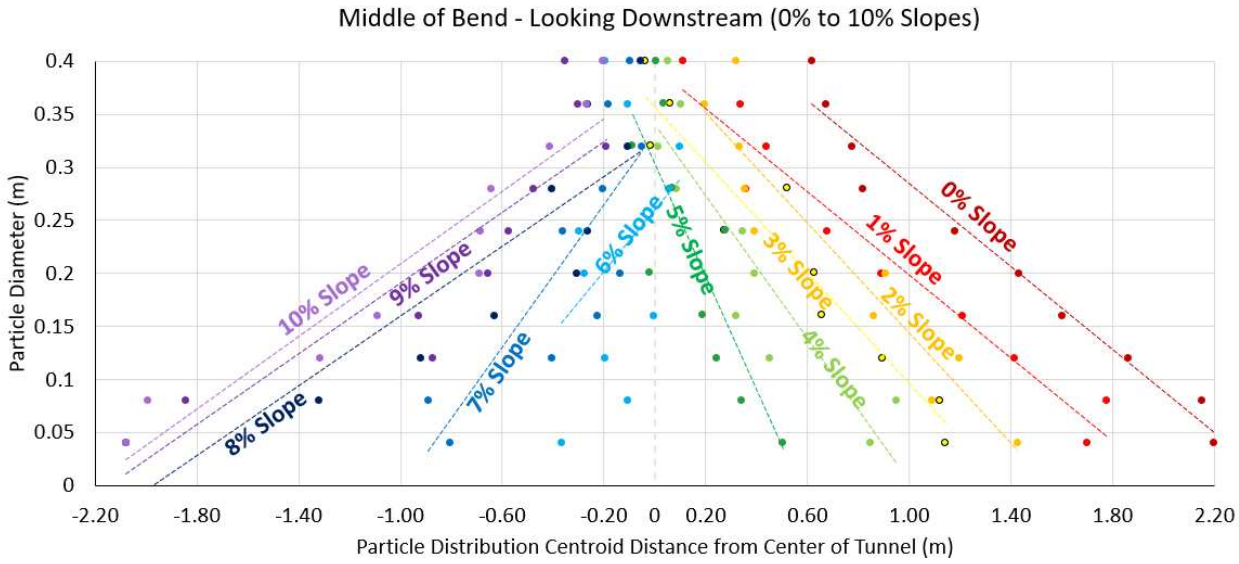

Figure 36. Summary of Particle Size and distance of centroid of particle distribution from center of SBT bend for 158.9 m^3/s. Middle of curve

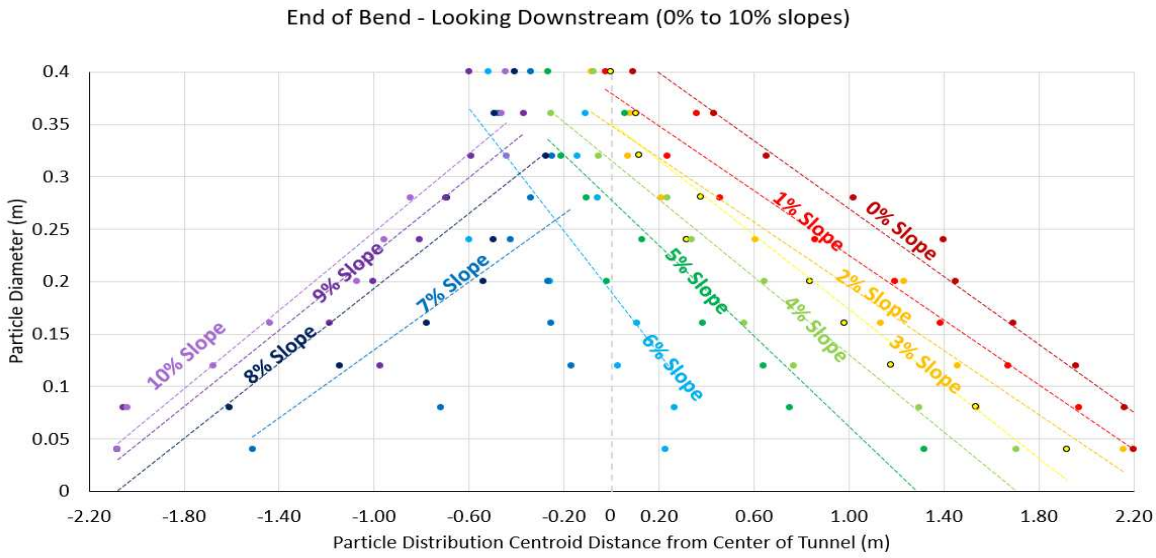

Figure 37. Summary of sediment-particle diameter and distance of centroid of particle distribution from center of SBT bend for 158.9 m3/s. End of curve or bend.

The Root Mean Square Error (RMSE) was calculated as a deviation from 0 (or the center of the tunnel). The further the center of the particle distribution is from the center of the SBT bend, the larger the error. Of the alternatives analyzed, the average of all data is summarized in the black line seen in Figure 38, which shows that a transverse slope between 4-6% produced the least amount of error.

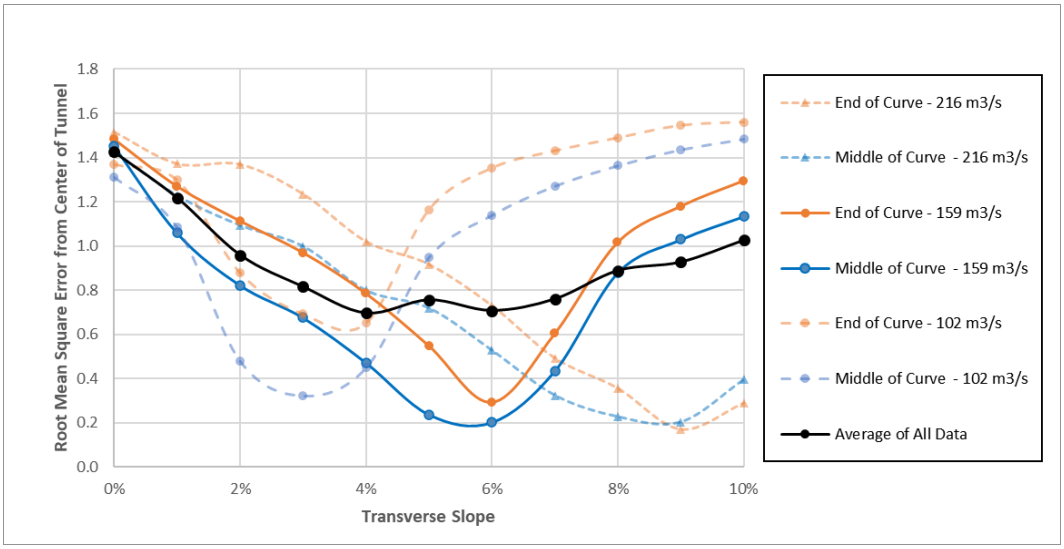

Figure 38. RMSE of how far the center of the particle-diameter distributions deviated from the center of the of the SBT cross-section.

The linear slope of the particle distributions was also calculated, using the equation of a line, where y = mx + b, and where m is the slope of the line. The linear fit function was used on each distribution in excel, and the m value was extracted from the equation of a line for each distribution. It is assumed that a slope closest to or parallel to the transverse slope indicates a particle distribution that is most evenly distributed across the invert of the tunnel. Figure 39 shows a black line which averages all the data, and predicts that a transverse slope betwee 2% and 4% might most evenly distribute the particles.

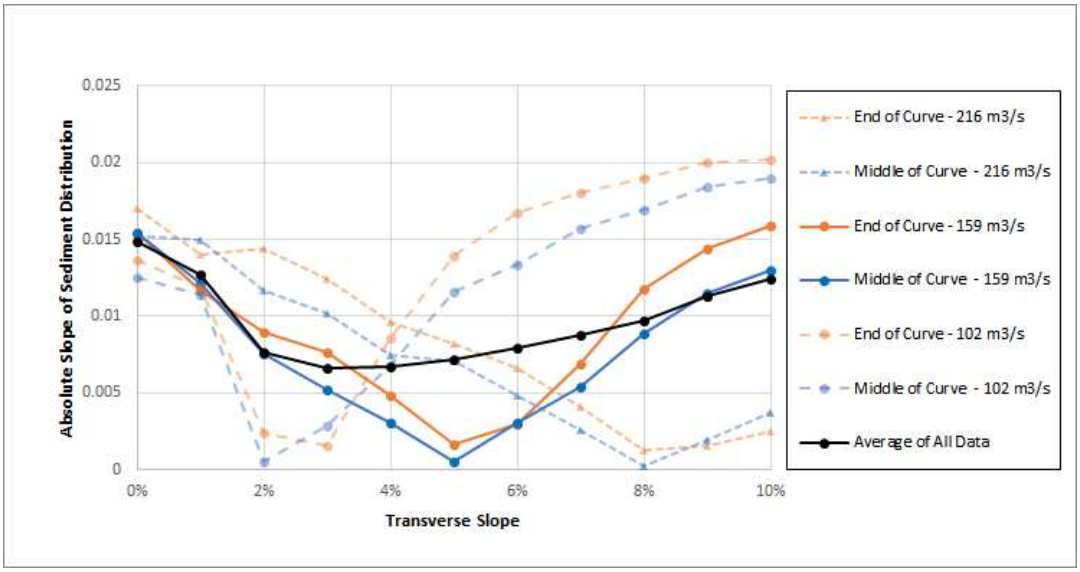

Figure 39. Absolute slope |m| of the particle distribution from a linear trend line (y = mx + b).

The CFD-DEM model predicts that larger particle sizes have less tendency to concentrate along the inside bend and are less influenced by the secondary current. This phenomenon may require further analysis in physical modeling to confirm. The transverse shear stresses were extracted from the model, averaged, and then converted into the dimensionless Shield's parameter for each grain size. When the Shield's parameters are plotted against existing criteria for critical Shield's parameter, the data appear to trend with values of critical Shield's parameter (see Figure 40). For instance, the smaller particles are more influenced by the secondary current velocities, and start to move toward the inside bend, and the larger particles are less influenced. For a particle size of 0.4 m, the Shields parameter does not exceed the critical value of the Shield's parameter estimated by Auel et al. (2017a) of 0.005, and as can be seen in Figure 36 and Figure 37, the larger particles do not shift as much due to the influence of the secondary current. Therefore, the model appears to be in good agreement with existing literature of critical Shield's parameter for fixed planar beds.

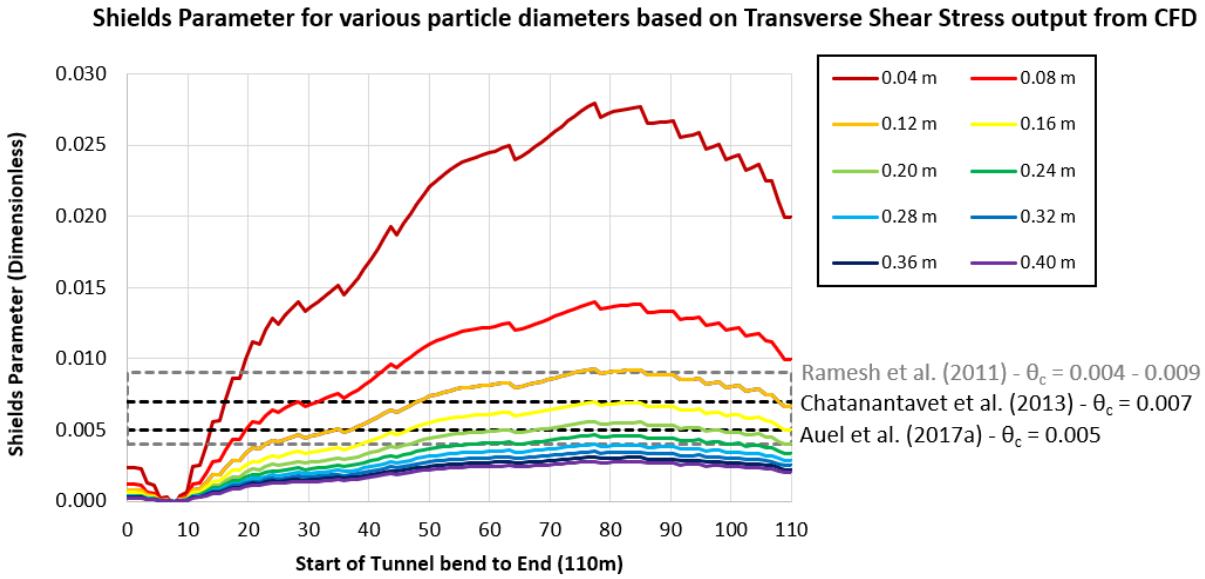

Figure 40. Shields parameters calculated from transverse shear stressed in CFD model, based on particle sizes, and compared to existing literature for critical shields parameter for fixed planar beds. (Chatanatavet 2013, Ramesh 2011, Auel et al. 2017).

What is not fully clear from this modeling, is why the smaller particles are more influenced by the transverse slope than are the larger particles. As can be seen in Figure 41, the velocities and corresponding transverse shear stresses vary across the invert of the tunnel. It is possible that the primary flow more greatly affected the larger particles. Also, possibly the smaller particles get funneled to the outside bend where they stay in the low velocity zone along the outside bend, close to the invert and wall and are less likely to be impacted by the secondary current, notably by transverse slopes greater than 5%. Larger particles protrude more into the flow, and experience more drag due to the secondary current. An intermediate range of particle sizes experience more impactful inter-particle collisions, and the collisions keep them more evenly spaced. Further study may be warranted to evaluate why particles finer than 0.04 m in diameter

concentrate to the outside bend, inside bend, and even concentrate to locations along the invert of the tunnel for the transverse slopes.

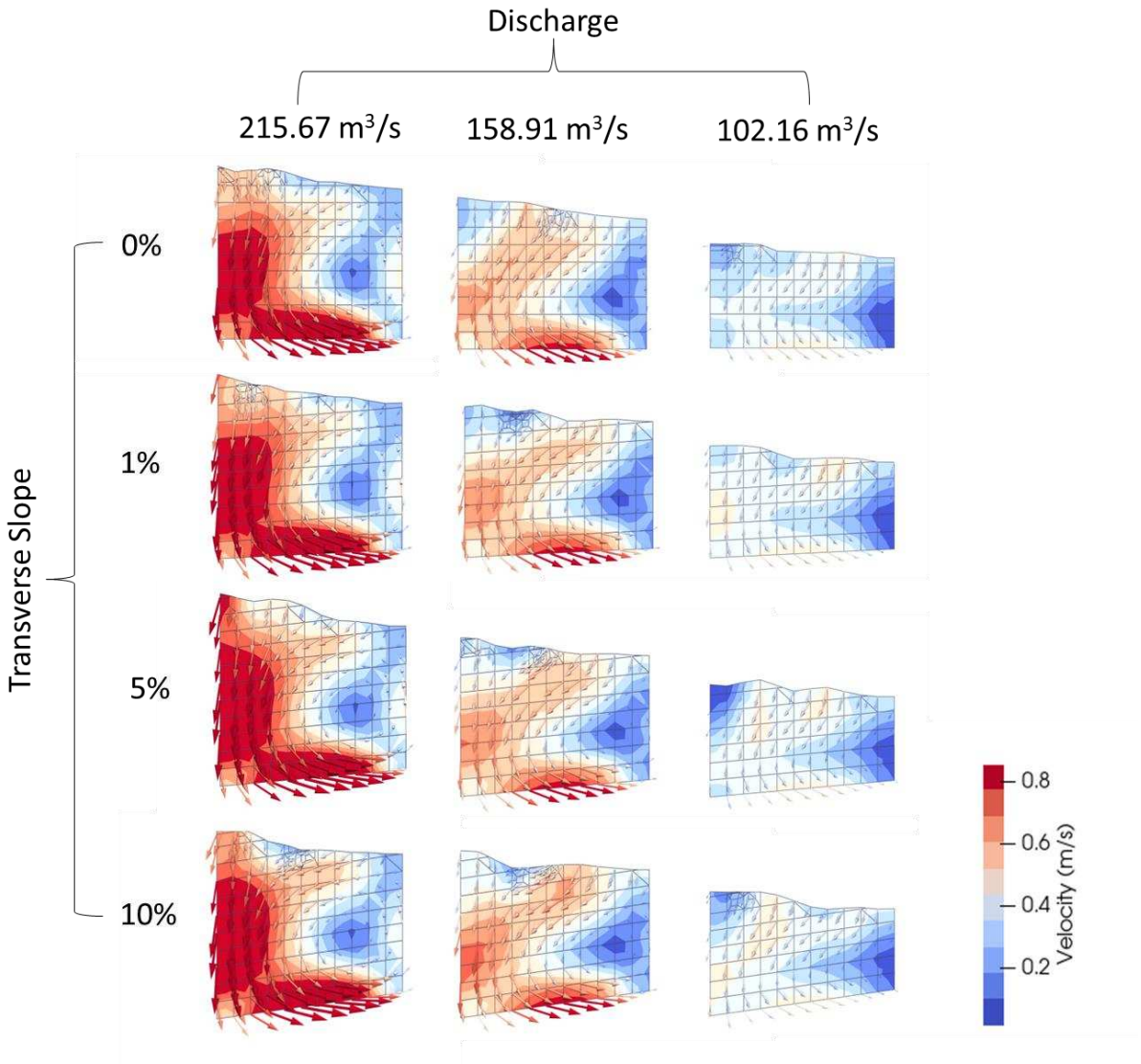

Figure 41. Transverse Velocities for Middle of Curve looking downstream for all the simulated discharges (215.67 m^3/s, 158.91 m^3/s and 102.16 m^3/s).

A more comprehensive summary of the data is shown in Figure 42 and Figure 43. The summary shows all the flows evaluated and summarizes the particle distributions at the middle of the bend.

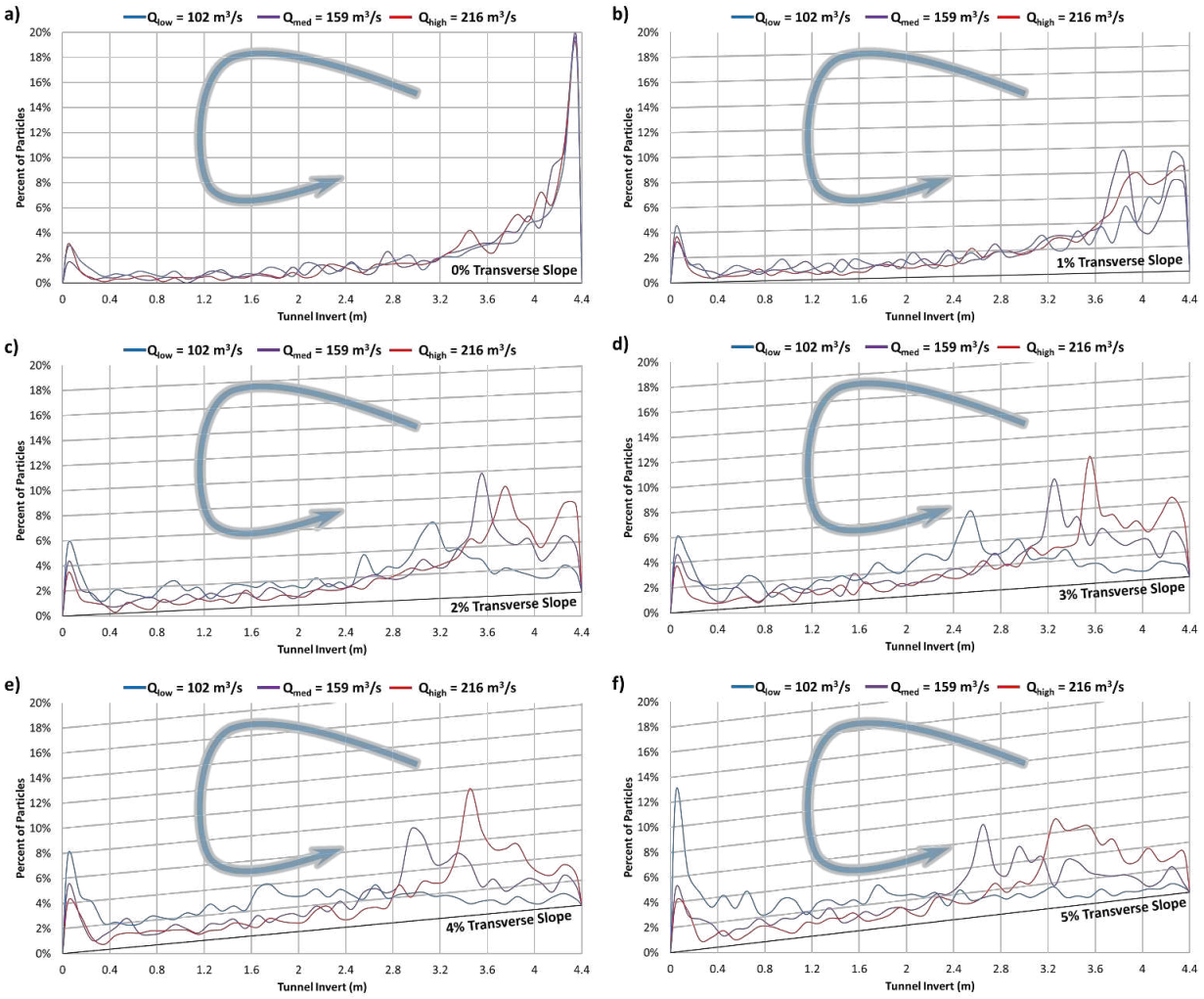

Figure 42. Summary of simulations at Middle of Curve (Q_{low} = 102.16 m^3/s, Q_{med} = 158.91 m^3/s and Q_{high} = 215.67 m^3/s). The Y-axis is augmented to match transverse slope for each alternative [0% to 5%, or a) to f) respectively] and illustrated with secondary current to help visualize how both impact sediment distribution.

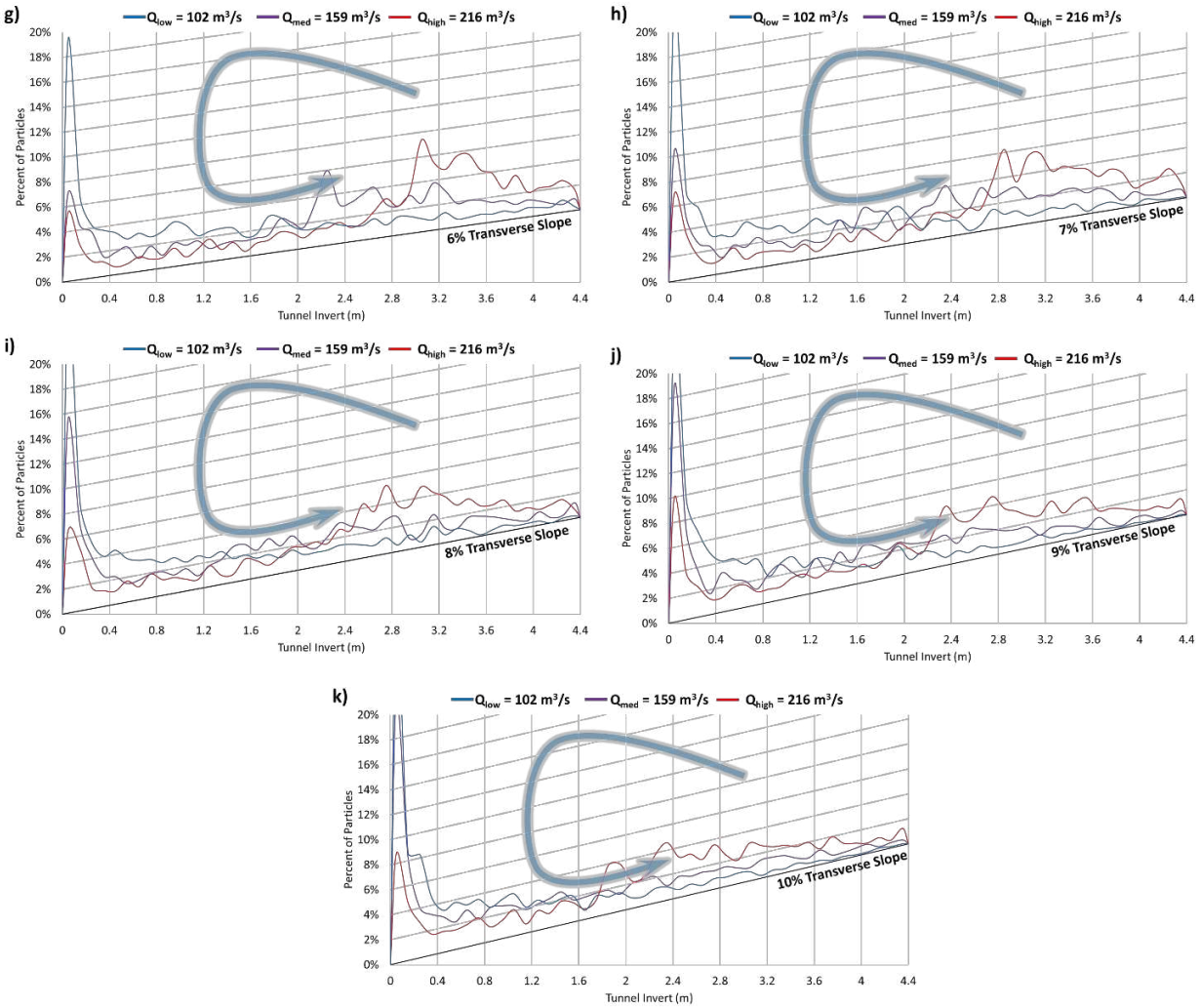

Figure 43. Summary of all simulations (Q_{low} = 102.16 m^3/s, Q_{med} = 158.91 m^3/s and Q_{high} = 215.67 m^3/s). Y axis is augmented to match transverse slope for each alternative [6% to 10%, or g) to k), respectively] and illustrated with secondary current to help visualize how both impact sediment distribution.

As can be seen in Figure *7*, the abrasion damage concentrates towards the inside bend of the Solis SBT. However, as can be seen in Figure 26 through Figure 30, the CFD-DEM predicts that larger sediment sizes can distribute across the entire invert. In the prototype tunnel that has been in operation since 2012, damage is only prevalent along the inside bend of the curve. This

finding may suggest that the SBT does not often experience particle sizes larger than those that the CFD-DEM model shows that concentrate near the bend's inner bank.

There was no appreciable difference between the transverse shear stresses on the bed between the transverse slope alternatives. An output from *ParaView* (v5.6.2) of the transverse shear stresses converted to the Shield's parameter using Eq 4 was created to examine the impact of the transverse sloping of the invert on the transverse shear stresses between the 0%, 5%, 20% and -20% transverse slopes. The -20% is a typical transverse slope seen in super-elevated or banked channels. As can be seen in Figure 44, except for the locations of the transition ramps, there is no appreciable difference between these transverse slopes. This result indicates that the strength of the secondary current is not impacted by the transverse slope alternatives and that each alternative produces the same magnitudes of transverse shear stress on the bed. Also shown in Figure 44 are the typical critical values of Shields stress found in the literature for fixed planar beds of particles.

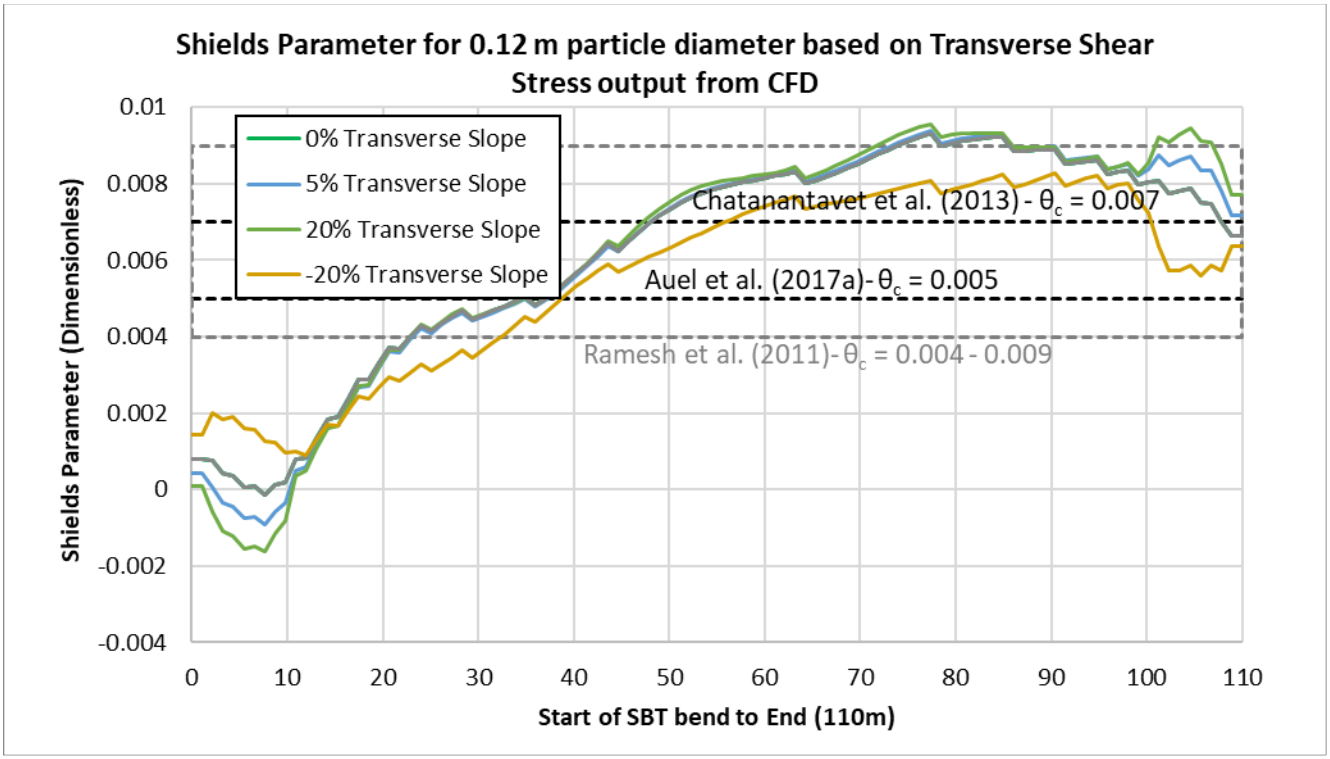

Figure 44. Comparison of transverse shear stresses along tunnel invert for 0%, 5%, 20% and -20% transverse slopes for 158.9 m^3/s flow.

A set of runs for each transverse slope was also completed with 40 particles that have a diameter of 0.12 m and the SBT conveys a flow of 158.9 m^3/s. A 0.12 m particle size was selected because according to the transport-mode criteria in Raudkivi (1998). In accordance with the criteria, and the discharge given, this particle size has a high likelihood of saltation. Also, according to the sediment grain distribution for the Solis SBT, it is a particle size that is prevalent in the tunnel. The CFD-DEM modeling shows the particle size is influenced by the secondary current. The width of sediment distribution was quantified visually for each alternative at the midpoint of the tunnel bend and at the end of the tunnel bend (see Figure 45). The sediment begins to spread more evenly across the invert as the transverse slope increases from 0% to 3%. From 3% to 5% the width stays constant but the moves away from the inside

bend and toward the outside of the bend. There is a fluctuation in the sediment width at 6% and 7%, and the sediment begins to focus into the outside bend as the width begins to reduce again for slopes between 7% and 10%. The results for the 6% and 7% slopes do not trend with the other transverse slope alternatives. This effect may be due to the random distribution of sediment at the inlet causing a local increase in this area. Although each simulation starts with the same sediment configuration, this sediment configuration may not disperse to the same degree for the 6% and 7% alternatives. Or this result may be due to the secondary current forces beginning to see a decrease in the threshold at which they can move sediment up the transverse slope, and the sediment is starting to gravitate to the outside bend.

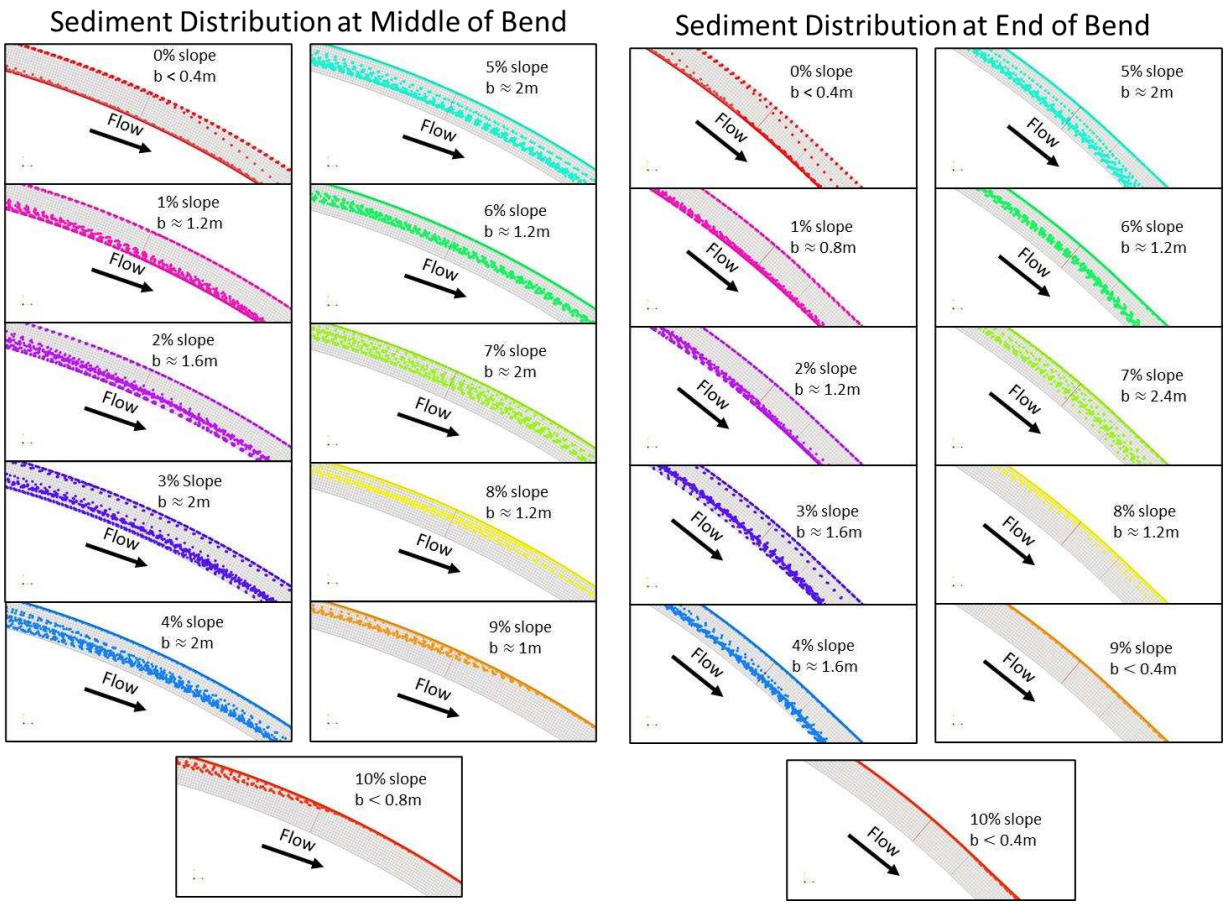

Figure 45. Sediment concentration widths (bottom width = b) analyzed in simulation of 40 particles of 0.12 m diameter with 158.91 m^3/s flow.

The corresponding change in abrasion rate can be seen in Table 5 below. To analyze the impact on abrasion, the q_s (unit gravimetric sediment supply rate) term based on the unit width of the tunnel can be used to quantify the impact on abrasion. The q_s term which has units of kg/(m·s), is the sediment supply rate divided by the width of the tunnel. The width of the tunnel is 4.4ft. However, this width assumes that the sediment is spread across the entire invert of the tunnel. When the sediment concentrates to the inside bend due to the secondary current, the sediment width narrows, and the entire sediment supply rate passes through a much smaller width. In the case of this analysis, the width narrowed as much as 0.2m. Therefore, if the sediment width is

only 0.2m then the sediment supply rate value would change from being divided by 4.4 being divided by 0.2. This narrowing would increase the sediment abrasion rate by at least 2,200% (4.4/0.2) along the inside corner of the bend.

Table 5. Abrasion rate increases due to concentrated width of sediment distribution in simulation with 40 particles, 0.12 m diameter, conveyed by 158.91 m^3/s of flow.

Transverse Slope	Width of Sediment Distribution (m)		Increase in Abrasion Rate	
	Middle	End	Middle	End
0%	0.2	0.2	2200%	2200%
1%	1.2	0.8	367%	550%
2%	1.6	1.2	275%	367%
3%	2	1.6	220%	275%
4%	2	1.6	220%	275%
5%	2	2	220%	220%
6%	1.2	1.2	367%	367%
7%	2	2.4	220%	183%
8%	1.2	1.2	367%	367%
9%	1	0.4	440%	1100%
10%	0.8	0.2	550%	2200%

The concentration of abrasion to within 0.2 m of the inside bend matches well with the photographs taken of the Solis SBT in 2024 (see Figure 46), for which 0.5 m near the inside bend of the 4.4m width tunnel invert appears to have concentrated abrasion. The abrasion is beginning to create an incision channel that is deepening and widening. Before deepening and widening, the abrasion area may have started closer to 0.2 m width, as suggested by the CFD-DEM modeling, then widened and deepened as the abrasion progressed.

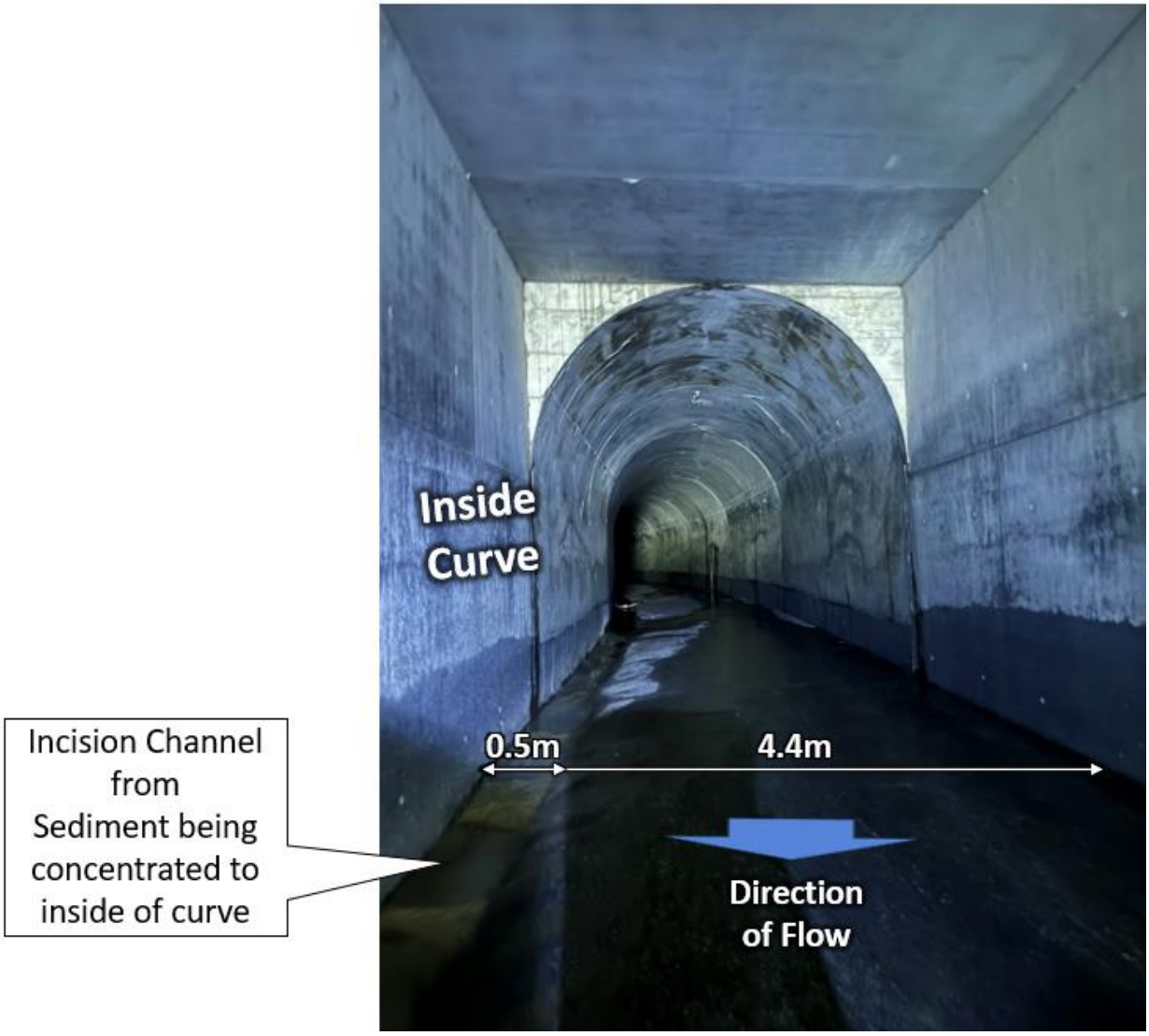

Figure 46. Looking upstream of the Solis SBT, with the abrasion concentrated along the inside bend of the SBT bend.

CHAPTER 5. CONCLUSIONS

5.1 Conclusions

The following main conclusions can be drawn from this study involving numerical (CFD-DEM) modeling of super-critical flow and associated sediment transport in a Sediment Bypass Tunnel (SBT), with Solis SBT used as the prototype example:

1. This study shows that secondary flows influence the distribution of sediment in SBTs by causing sediment particles, especially saltating particles, to move toward the inner bank of a SBT bend. The near-bed portion of the secondary current in a bend is directed toward the inner bank.
2. A small amount of transverse sloping (1% to 2% extending upwards from the outerbank) of the invert of an SBT bend benefited all flow scenarios modelled, doing so by causing sediment particles to be more evenly distributed across the bend's invert. If implemented, the slope should be field monitored closely to determine if indeed abrasion patterns reduce. These transverse slopes are modest, in consequence of the variation of invert roughness and bend angle. Roughness variation was simulated implicitly by the numerical model.
3. When designing the transverse slope for an existing SBT or a proposed SBT, important factors to consider are the target sediment size (determined as the mean particle size or the particle most likely to saltate), the target flow, the SBT slope, the primary and the transverse shear stresses on the SBT invert, SBT bend angle, and how gradually the 0% level transverse invert of the straight approach channel transitions to the transverse slope of the invert of a channel bend, and how gradually the bend invert slope should occur

downstream of the bend when the channel becomes straight again. No bedforms, notably antidunes, form in the SBT.

4. The influence of the secondary current continues downstream of the SBT bend for some distance as can be seen in Figure 18. For the SBT at the Solis Reservoir (Switzerland), for over at least another 50 m, downstream of the bend, the secondary current influenced the path of the particles. Also, for the flow ranges simulated, there is no explicit equalizing effect of transverse shear stresses to move the particles back to the center of the channel after the secondary currents have moved them toward the inside of the SBT bend, except for interparticle collisions and turbulent mixing. Therefore, continuing the transverse sloping downstream of the SBT bend may distribute the sediment more evenly after the bend. Further research is required to determine how to gradually transition the transverse sloping of the bend to the downstream 0% transverse slope invert of a straight channel.
5. The smaller particles are more influenced by the transverse sloping and secondary current, likely because the smaller particles travel through the tunnel slower than the large particles and are susceptible to the forces of the secondary current and/or transverse sloping for a longer time. Too much transverse sloping concentrates all particle sizes along the outside bank of a bend.
6. The bottom width, b, to height, h, ratio of the flow (b/h ratio) evaluated in this study varied between 1.2 and 2. For a fixed bend radius, as the ratio increased the strength of the secondary current decreased because the greater contact of the secondary current with the invert. However, b/h ratios out of this range likely produce secondary current patterns that distribute sediment differently across the invert.

A CFD model, even if not coupled with a DEM model, could still provide useful insight into the transverse shear stresses along the tunnel bend. For example, as demonstrated with Figure 40, the transverse shear stresses and calculated Shield's parameter for various grain sizes correlate well with the model results. In addition to the shear stresses generated by the streamwise (primary) flow, if the transverse shear stresses exceed the Shield's parameter the particles move toward the inside of a bend.

5.2 Recommended Further Study

Recommended further study includes additional laboratory study to verify these results from numerical modeling. The laboratory study should evaluate (1) the behavior of the flow field generated by super-critical flow along a bend, and (2) particles transported through the flow field. Such studies will address these objectives and may confirm, or disprove, that transverse slopes obtained in this study.

Further studies also are needed to evaluate how far downstream the transverse sloping should extend, and how gradually it should be transitioned back to the 0% transverse slope. Additional CFD-DEM coupling modeling could also try to mimic the behavior of saltation, or a similar study could evaluate the influence of different particle shapes rather than spherical used in this study. A more gradual banking that more closely matches the increasing transverse shear stress could better distribute the sediment as it moves downstream. As can be seen in Figure *40*, the shields parameter (and transverse shear stress) increases gradually as flow progresses through the tunnel bend and then decreases gradually as flow exits the tunnel bend. Analysis could also be done to evaluate if sediment is best distributed when the transverse slope increases and decreases gradually at the same rate as the transverse shear stress.

A hypothesis for the increased abrasion rate on the inside bend in the Mud Mountain SBT is that segregation of the bedload into the most saltation prone sizes may increase the abrasion rate on the inside bend. From examining the output from the CFD-DEM model it is possible that the concentration of sediment to the inside bends creates more opportunity for interparticle collisions, increasing the amount of saltating particles and abrasion. As observed in the physical model for Solis and the CFD-DEM modeling, larger particles travel faster in the tunnel and can be set into saltation when colliding with smaller particles. Further analysis may be warranted to determine why the volume loss increases due to the secondary current, instead of matching the volume loss of the downstream tunnel.

REFERENCES

Abbott, J. E., & Francis, J. R. D. (1977). Saltation and suspension trajectories of solid grains in a water stream. Philosophical Transactions of the Royal Society of London. Series A, Mathematical and Physical Sciences, 284(1321), 225–254. https://doi.org/10.1098/rsta.1977.0009.

Alice Hager, Christoph Kloss, Christoph Goniva, Combining, 2018,Open Source and Easy Access in the field of DEM and coupled CFD-DEM: LIGGGHTS®, CFDEM®coupling and CFDEM®workbench, https://doi.org/10.1016/B978-0-444-64235-6.50296-5

Ancey, C., Bigillon, F., Frey, P., Lanier, J., & Ducret, R. (2002). Saltating motion of a bead in a rapid water stream. Physical Review E, 66(3), 036306. https://doi.org/10.1103/PhysRevE.66.036306.

Auel, C. (2014). Flow characteristics, particle motion and invert abrasion in sediment bypass tunnels. VAW-Mitteilungen 229 (R. Boes, ed.), PhD Thesis, ETH Zurich, Switzerland.

Auel, C., Albayrak, I., & Boes, R. M. (2014). Turbulence characteristics in super-critical open channel flows: Effects of Froude number and aspect ratio. Journal of Hydraulic Engineering, 140(4), 04014004. https://doi.org/10.1061/(ASCE)HY.1943-7900.0000841.

Auel, C., Albayrak, I., Sumi, T., & Boes, R. M. (2017a). Sediment transport in high-speed flows over a fixed bed: 1. Particle dynamics. Earth Surface Processes and Landforms, 42(9), 1365–1383. https://doi.org/10.1002/esp.4128.

Auel, C., Albayrak, I., Sumi, T., & Boes, R. M. (2017b). Sediment transport in high-speed flows over a fixed bed: 2. Particle impacts and abrasion prediction. Earth Surface Processes and Landforms, 42(9), 1384–1396. https://doi.org/10.1002/esp.4132.

Auel, C., & Boes, R. M. (2011). Sediment bypass tunnel design-review and outlook. Proc. ICOLD Symposium "Dams under changing challenges" (A. J. Schleiss & R. M. Boes, eds.), 79th Annual Meeting, Lucerne, Switzerland: 403-412.

Blanckaert and Vriend, J. Fluid Mech. (2004) Secondary Flow in sharp open-channel Bends.

Chatanantavet, P., Whipple, K. X., Adams, M. A., & Lamb, M. P. (2013). Experimental study on coarse grain saltation dynamics in bedrock channels. Journal of Geophysical Research: Earth Surface, 118(2), 1161–1176. https://doi.org/10.1002/jgrf.20053.

Chow, V. T. (1959). Open-channel hydraulics. McGraw-Hill.

Demiral, D., Boes, R. M. & Albayrak, I. Effects of secondary currents on turbulence characteristics of super-critical open channel flows at low aspect ratios. *Water* **12**, 3233. https://doi.org/10.3390/w12113233 (2020).

F.F. Dizaji, J.S. Marshall, J.R. Grant, Collision and breakup of fractal particle agglomerate in a shear flow, Journal of Fluid Mechanics, 862 (2019) 592-623. https://doi.org/10.1017/jfm.2018.959.

Francis, J. R. D., & Bagnold, R. A. (1973). Experiments on the motion of solitary grains along the bed of a water-stream. Proc. Royal Society of London. A. Mathematical and Physical Sciences, 332(1591), 443–471. https://doi.org/10.1098/rspa.1973.0037.

Hager, W.H., Schleiss, A.J., Boes, R.M., Pfister, M. (2020). Hydraulic Engineering of Dams. Taylor & Francis, London, https://doi.org/10.1201/9780203771433.

Henderson, F.M. (1966). Open channel flow. Macmillan, New York, NY.

Hu, C., & Hui, Y. (1996a). Bed-load transport. I: Mechanical characteristics. Journal of Hydraulic Engineering, 122(5), 245–254. https://doi.org/10.1061/(ASCE)0733-9429(1996)122:5(245).

Ippen, A. T. An analytical and experimental study of high velocity flow in curved sections of open channels, Doctoral Thesis. California Inst. Technol. https:// doi. org/ 10. 7907/ 162E- WA65 (1936).

Jaiswal, A., Bui, M. D., & Rutschmann, P. (2023). On the process of fine sediment infiltration into static gravel bed: A CFD–DEM modelling perspective. River Research and Applications, 1–20. https://doi.org/10.1002/rra.4215

Kitanidis, P. K., & Kennedy, J. F. (1984). Secondary current and river-meander formation. Journal of Fluid Mechanics, 144, 95–114. https://doi.org/10.1017/S0022112084001595

Knapp, R. T. High-velocity flow in open channels: A symposium: Design of channel curves for super-critical flow. Trans. Am. Soc. Civ. Eng. 116, 296–325. https:// doi. org/ 10. 1061/ TACEAT. 00065 30 (1951)

LIGGGHTS. (2024). LIGGGHTS: Open Source Discrete Element Method Particle Simulation Code. [Online] Available at: https://www.cfdem.com/liggghts

Liu, Q., Andersen, L. V., Zhang, M., & Wu, M. (2024). Abrasion damage of concrete for hydraulic structures and mitigation measures: A comprehensive review. Construction and Building Material

M. Facchini, Hydroabrasion in high-speed flow at sediment bypass tunnels, ETH Zürich, 2017.

Mud Mountain LiDAR Scan Final Report 2023, US Army Corps of Engineers

Müller-Hagmann, M. (2017). Hydroabrasion by high-speed sediment-laden lows in sediment bypass tunnels. VAW-Mitteilungen 239 (R. Boes, ed.), PhD Thesis, ETH Zurich, Switzerland.

Odgaard, A. J., & Kennedy, J. F. (1983). River-bend bank protection by submerged vanes. Journal of Hydraulic Engineering, 109(8), 1161-1173. https://doi.org/10.1061/(ASCE)0733-9429(1983)109:8(1161)

OpenFOAM. (2019). OpenFOAM documentation. *OpenFOAM Foundation. Retrieved from https://www.openfoam.com/documentation/guides/latest/doc/index.html*

Philippe Traoré, Jean-Charles Laurentie, Lucian Dascalescu, An efficient 4 way coupling CFD–DEM model for dense gas–solid particulate flows simulations, Computers & Fluids, Volume 113, 2015, Pages 65-76, ISSN 0045-7930, https://doi.org/10.1016/j.compfluid.2014.07.017.

Prandtl, L. *Essentials of Fluid Dynamics* (Blackie and Son, 1952).

Shields, A. (1936). "Application of similarity principles and turbulence research to bed-load movement".

Sklar, L. S., & Dietrich, W. E. (2004). A mechanistic model for river incision into bedrock by saltating bed load. Water Resources Research, 40(6). https://doi.org/10.1029/2003WR002496.

Solis Physical Model Report, 2010, VAW 4269

Raudkivi, A. J. (1998). *Loose Boundary Hydraulics* (4th ed.). Rotterdam: A.A. Balkema.

Ramesh, B., Kothyari, U. C., & Murugesan, K. (2011). Near-bed particle motion over transitionally- rough bed. Journal of Hydraulic Research, 49(6), 757–765. https://doi.org/10.1080/00221686.2011.620369.

Rouse, H. (Ed.). (1950). Engineering Hydraulics. Wiley, New York.